Engineering Analysis with Boundary Elements 156 (2023) 223–238

Contents lists available at ScienceDirect

Engineering Analysis with Boundary Elements

journal homepage: www.elsevier.com/locate/enganabound

# Implicit differentiation-based reliability analysis for shallow shell structures with the Boundary Element Method

Mengke Zhuang [a,*], Llewellyn Morse [b], Zahra Sharif Khodaei [a], M.H. Aliabadi [a]

[a] Department of Aeronautics, Imperial College London, South Kensington Campus, City and Guilds Building, Exhibition Road, SW7 2AZ, London, UK
[b] Department of Mechanical Engineering, University College London, Roberts Building, WC1E 6BT, London, UK

ARTICLE INFO

*Keywords:*
Shallow shell structure
First-Order Reliability Method (FORM)
Boundary Element Method (BEM)
Sensitivity analysis
Optimisation

ABSTRACT

A novel methodology for evaluating the response sensitivities of shallow shell structures using the Boundary Element Method (BEM) is presented in this work. The implicit derivatives of the BEM formulations for shallow shell structures, with respect to the geometrical variables, such as curvature and thickness, have been derived for the first time and incorporated into an Implicit Differentiation Method (IDM). The IDM is employed in conjunction with the First Order Reliability Method (FORM) to evaluate the reliability of shallow shell structures. The accuracy of the IDM formulation is first validated against an analytical solution, with results showing a maximum difference of only 2.61%. The IDM was later validated against the Finite Difference Method (FDM), with results showing a maximum difference of only 0.11%. The IDM was also found to be significantly more efficient than the FDM, requiring 35% less CPU time when calculating sensitivities. This is further compounded by the fact that, unlike the FDM, the IDM does not require a step size. A numerical example featuring a circular shallow shell is used to demonstrate the application of the IDM-based FORM for assessing structural reliability. The uncertainty in curvature is set as a variable for the purpose of investigating its impact on reliability. The results of the reliability index obtained from the IDM-FORM are compared to the results obtained from FDM-FORM and were found to be very similar. An analysis of sensitivity is conducted to identify the most significant variables affecting reliability. It is found that uncertainties in curvature, thickness, and applied pressure distribution parameters have the largest impact on structural reliability. To demonstrate how the IDM could be used in practice, it was employed as gradient-based optimisation procedure featuring shallow-shell structures. The IDM was found to be a very efficient and accurate alternative to existing methods for calculating structural response sensitivities.

## 1. Introduction

In general, every engineering parameter has a certain level of uncertainty associated with its value. These uncertainties might come from sources such as human error, environmental factors, or imperfect manufacturing processes, and failure to consider these uncertainties might lead to catastrophic failure of a structure. The conventional method of defining structural safety involves the use of safety factors to prevent structural failure. As a result of this conservative approach, structures can become over-engineered, since parameters are often treated in a deterministic manner.

Reliability analysis offer an alternative to this deterministic approach and has been developed based on the mathematical and probabilistic theory. Structural safety can be found through the calculation of the reliability index, which is a measurement of the probability of failure. In reliability analysis, parameters are treated in a non-deterministic manner that considers both the effect of the parameters' mean as well as the variance in determining structural reliability [1]. Reliability analysis has been applied extensively to reliability-based optimisation problems, and sensitivity analysis, which allows engineers to identify the most critical design factor based on design constraints. Several methods can be used to evaluate the reliability index, including Monte Carlo Simulation (MCS), First-Order Reliability Method (FORM) and Second-Order Reliability Method (SORM). MCS is used for solving stochastic simulations that involve a large amount of random sampling. FORM and SORM, on the other hand, rely on approximating the Limit State Function (LSF), which is a function that defines the boundary between the failure and safety regions of a structure. In the FORM, the LSF is approximated using a first-order Taylor expansion, while in

* Corresponding author.
*E-mail addresses:* m.zhuang17@imperial.ac.uk (M. Zhuang), l.morse@ucl.ac.uk (L. Morse), z.sharif-khodaei@imperial.ac.uk (Z. Sharif Khodaei), m.h.aliabadi@imperial.ac.uk (M.H. Aliabadi).

https://doi.org/10.1016/j.enganabound.2023.07.041
Received 15 March 2023; Received in revised form 28 July 2023; Accepted 28 July 2023
Available online 15 August 2023

the SORM, it is approximated using a second-order Taylor expansion. Details of these methods can be found in [2]. FORM is used in this study to evaluate the reliability index of a structure, thus predicting the probability of failure.

In the field of reliability analysis with the FORM, the Finite Element Method (FEM) has been widely used [3,4]. The Boundary Element Method (BEM), due to its advantages related to dimension reduction, has also become increasingly popular in recent decades. The BEM requires only the outer boundaries of the structure to be modelled, thereby reducing the dimension of the system. The combination of reliability analysis and the BEM has been used in several applications, including sensitivity problems in an acoustic system [5], evaluating the heat impact sensitivity of metal [6], and solving contact problems [7,8], as well as plate bending problems [9]. In [10] the Advanced First-Order Second Moment (AFOSM) was applied to solve 2D elastic problems with analytically evaluated sensitivities. Reliability analysis has also been widely applied to shape optimisation problems incorporating the BEM, such as topology optimisation problems [11] and 2D anisotropic shape optimisation problems [12].

When calculating the probability of failure, the FORM requires the sensitivities of the response of the structure to changes in design variables or loading conditions. In rare instances, the derivatives or sensitivities can be found by the explicit derivation of the expression of the limit state function [13,14]. Generally, the derivatives are determined using numerical methods. The derivatives have been evaluated using a variety of approaches, including linearising the limit state function and performing a duplicate Monte Carlo simulation or using a surrogate model [15]. In [16], the derivatives were evaluated using the Finite Difference Method (FDM) and the Probabilistic Finite Element Method (PFEM). The Implicit Differentiation Method (IDM) has been developed in [17] to provide analytical derivatives of boundary integral equations in BE. Examples can be found in [18–20].

Notable work on the application of the BEM for reliability analysis using MCS and FORM can be found in [18] where reliability analysis was conducted on a 2D electrostatic rectangular plate with a centre hole subjected to uni-axial loading. The first-order sensitivities were calculated using the Implicit Differentiation Method (IDM). Good agreement was found between the results obtained from the FORM and the results obtained from MCS. The uncertainties in the material properties and geometrical variables were taken into account. Similar examples can be found in [20] with the application to the shape optimisation of plate structures [21].

Modern engineering structures can often be modelled as shell structures. These include cylindrical walls, domes, and aircraft fuselages. Shell structures are often superior to flat plates in withstanding high loads, since the shell structure mostly experiences membrane loading, whilst also remaining lightweight. In particular, thin/shallow shells are widely applied due to their low weight. Among the literature, the use of reliability analysis with the BEM for shell structures has been scarcely investigated. Some examples of the work pertaining to shell structure-related reliability are, for example, [22] for the shell truss structure using the MCS, [23] for a pressurised shell incorporating surrogate modelling and reliability analysis, and [24] for a laminate composite shell. The most relevant work was conducted on a plate structure with the BEM in [25] for plate bending problems and assembled plate structures in [26]. There have not yet been any works involving the reliability analysis of shell structures using the BEM.

The main novelty of this current work is that the direct derivatives of the BEM formulations for shallow-shell structures have been derived for the first time and formulated as part of an IDM. The IDM, combined with the advantages of the BEM, can be a very efficient tool for structural reliability analysis. To validate the IDM, the structural response sensitivities obtained from the IDM for a shell structure will be compared with the sensitivities obtained by an analytical solution and sensitivities obtained by the FDM. Another novelty is the reliability analyses conducted for a more complex shell structure, whilst considering the uncertainties in the geometry, material properties, and loading conditions. Both the IDM and the FDM will be used to evaluate the reliability index.

The layout of the paper is as follows: The methodology of the BEM formulations and their derivatives are presented in Section 2. Verification of the proposed derivatives is given in Section 3 where the IDM is compared against an analytical example featuring a hemispherical dome. A more complex shell structure was used for the reliability analysis in Section 4 and the results of the sensitivity analysis are presented. Based on the results given by the sensitivity analysis, in Section 5, an optimisation procedure was performed. A second numerical example involving more geometrical parameters was used with Reliability-based Design Optimization (RBDO) to further illustrate possible practical applications of the BEM-IDM formulations. Detailed derivatives of the DRM method and BEM formulations are given in the Appendices.

## 2. Methodology

In this section, the shallow shell structure formulations for the BEM and the IDM are presented. A brief introduction to reliability analysis based on the Most-Probable Point (MPP) method is given.

Latin letter indexes (e.g. $i$, $j$, $k$) can take values of from 1 to 3 and Greek letter indexes (e.g. $\alpha$, $\beta$, $\phi$) can take values from 1 to 2.

### 2.1. BEM formulations for shallow shell structures

The classic theory of the shallow elastic shell can be found in [27]. Based upon the classic theory, Naghdi [28] and Reissner [29] developed shallow shell theory including transverses normal stress and shear deformation. The boundary integral equations were then developed by Lu and Huang [30] and the Dual Reciprocal method was introduced by [31] for transferring the domain integral equations to the boundary integral equations. This section introduces the BEM formulations developed for shallow shell structures, following work by [32].

The generalised displacement and tractions in this work are defined as $w_\alpha$ denote the rotations in the $x_1$ and $x_2$ directions ($\phi_{x1}$ and $\phi_{x2}$). $w_3$ denotes the out-of-plane displacement which is normal to the middle surface. $u_\alpha$ represents the in-plane displacements in the $x_1$ and $x_2$ directions ($u$ and $v$), respectively. $p_\alpha$ are the bending tractions due to the stress couples ($m_1$ and $m_2$), and $p_3$ is the shear traction due to the shear stress resultant ($t_3$). $t_1$ and $t_2$ denote the membrane tractions in the $x_1$ and $x_2$ directions, respectively. Details of these definitions are given in Fig. 1

Consider a shell structure with the principal curvatures $\kappa_{11} = 1/R_1$ and $\kappa_{22} = 1/R_2$, where $R_1$ and $R_2$ represent the radius of curvature of the shell in the $x_1$ and $x_2$ directions, respectively. From [32,33], the displacement integral equations for rotations, $w_1$ and $w_2$, and out-of-plane displacement, $w_3$, is:

$$
\begin{aligned}
&c_{ij}\left(x'\right) w_j\left(x'\right) + \int_\Gamma P^*_{ij}\left(x', x\right) w_j(x) d\Gamma(x) = \int_\Gamma W^*_{ij}\left(x', x\right) p_j(x) d\Gamma(x) \\
&- \int_\Omega W^*_{i3}\left(x', X\right) \kappa_{\alpha\beta} B \frac{1-\nu}{2} \\
&\times \left[u_{\alpha,\beta}(X) + u_{\beta,\alpha}(X) + \frac{2\nu}{1-\nu} u_{\phi,\phi}(X)\delta_{\alpha\beta}\right] d\Omega(X) \\
&- \int_\Omega W^*_{i3}\left(x', X\right) \kappa_{\alpha\beta} B \left((1-\nu)\kappa_{\alpha\beta} + \nu\delta_{\alpha\beta}\kappa_{\phi\phi}\right) w_3(X) d\Omega(X) \\
&+ \int_\Omega W^*_{i3}\left(x', X\right) q_3(X) d\Omega(X)
\end{aligned}
\tag{1}
$$

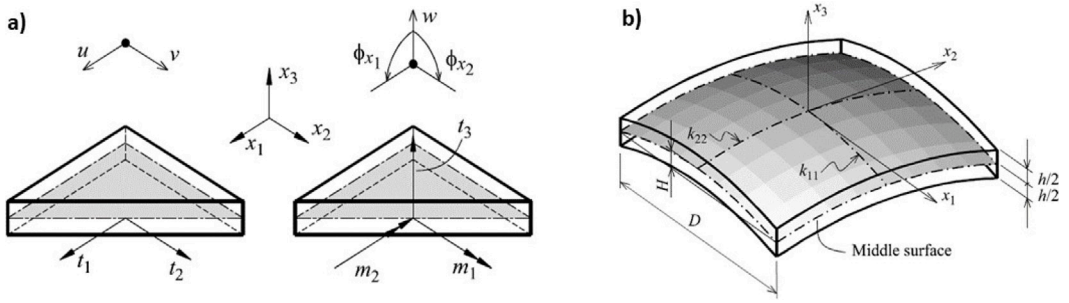


**Fig. 1.** Definition of the generalised displacements and tractions and the curvatures for the shell structure in the BEM [2].

and the displacement integral equations for in-plane displacements, $u_1$ and $u_2$, are:

$$\begin{aligned} & c_{\theta\alpha}\left(x'\right)u_{\alpha}\left(x'\right)+\int_{\Gamma}T_{\theta\alpha}^{*(i)}\left(x',x\right)u_{\alpha}(x)d\Gamma(x) \\ & +\int_{\Gamma}U_{\theta\alpha}^{*}\left(x',x\right)B\left[\kappa_{\alpha\beta}(1-\nu)+\nu\delta_{\alpha\beta}\kappa_{\phi\phi}\right]w_3(x)n_{\beta}(x)d\Gamma(x) \\ & -\int_{\Omega}U_{\theta\alpha}^{*}\left(x',X\right)B\left[\kappa_{\alpha\beta}(1-\nu)+\nu\delta_{\alpha\beta}\kappa_{\phi\phi}\right]w_{3,\beta}(X)d\Omega(X) \\ & =\int_{\Gamma}U_{\theta\alpha}^{*}\left(x',x\right)t_{\alpha}(x)d\Gamma(x)+\int_{\Omega}U_{\theta\alpha}^{*}\left(x',X\right)q_{\alpha}(X)d\Omega(X) \end{aligned} \tag{2}$$

with

$$c_{ij}(x')=\begin{cases}\frac{1}{2}\delta_{ij} & x'\in\Gamma\\ 1 & X'\in\Omega\end{cases} \tag{3}$$

where $f$ is the Cauchy principal value integral. $x'$ and $x$ denote the source and field points respectively. The tension stiffness is given by $B = Eh^3/[12(1-\nu)]$ is the tension stiffness, where $E$ is the Young's modulus, $h$ is the thickness of the shell and $\nu$ is the Poisson's ratio. $x \in \Gamma$ and $X \in \Omega$ represent the field points on the boundary and in the domain, respectively. $q_\alpha$ is the membrane body force, while $q_3$ is the domain pressure force. $n_\beta$ is the unit normal at the collocation point. $W_{ij}^*$ and $U_{\theta\alpha}^*$ are the displacement fundamental solutions, $P_{ij}^*$ and $T_{\theta\alpha}^{*(i)}$ are the traction fundamental solutions. Note that in both boundary integral equations, the integration is performed with respect to both the boundary $\Gamma$ and domain $\Omega$. The Dual Reciprocity Method (DRM) was used to transform the domain integrals to boundary integrals. Expressions for the fundamental solutions and particular solutions for the DRM can be found in [32].

The system of equations used in the BEM is expressed as $\mathbf{Hu} = \mathbf{Gt}$, with $\mathbf{H}$ and $\mathbf{G}$ denoting the coefficient matrix, where $\mathbf{u}$ and $\mathbf{t}$ contain known and unknown boundary displacements and tractions, respectively. Rearranging such that $\mathbf{X}$ contains all the unknowns and $\mathbf{F}$ contains all the known boundary displacements and tractions, allows the system of equations to be expressed as follows:

$$\mathbf{AX} = \mathbf{F} \tag{4}$$

### *2.2. BEM-IDM formulations for shallow shell structures with respect to a geometrical variable $Z_g$*

In this section, the BEM-IDM formulations for shallow shell structures with respect to some design variables are presented. The derivatives of the displacement integral equations (Eqs. (1)–(2)) with respect to a geometrical variable $Z_g$ (e.g. shell width, length, radius etc.) are:

$$\begin{aligned} & c_{ij}\left(x'\right)w_{j,g}\left(x'\right)+\int_{\Gamma}\left[P_{ij,g}^{*}\left(x',x\right)w_j(x)+P_{ij}^{*}\left(x',x\right)w_{j,g}(x)\right]d\Gamma(x) \\ & =\int_{\Gamma}\left[W_{ij,g}^{*}\left(x',x\right)p_j(x)+W_{ij}^{*}\left(x',x\right)p_{j,g}(x)d\Gamma(x)\right. \\ & -\int_{\Omega}W_{i3,g}^{*}\left(x',X\right)\kappa_{\alpha\beta}B\frac{1-\nu}{2} \\ & \times\left[u_{\alpha,\beta}(X)+u_{\beta,\alpha}(X)+\frac{2\nu}{1-\nu}u_{\phi,\phi}(X)\delta_{\alpha\beta}\right]d\Omega(X) \\ & -\int_{\Omega}W_{i3}^{*}\left(x',X\right)\kappa_{\alpha\beta}B\frac{1-\nu}{2} \\ & \times\left[u_{\alpha,\beta g}(X)+u_{\beta,\alpha g}(X)+\frac{2\nu}{1-\nu}u_{\phi,\phi g}(X)\delta_{\alpha\beta}\right]d\Omega(X) \\ & -\int_{\Omega}W_{i3,g}^{*}\left(x',X\right)\kappa_{\alpha\beta}B\left((1-\nu)\kappa_{\alpha\beta}+\nu\delta_{\alpha\beta}\kappa_{\phi\phi}\right)w_3(X)d\Omega(X) \\ & -\int_{\Omega}W_{i3}^{*}\left(x',X\right)\kappa_{\alpha\beta}B\left((1-\nu)\kappa_{\alpha\beta}+\nu\delta_{\alpha\beta}\kappa_{\phi\phi}\right)w_{3,g}(X)d\Omega(X) \\ & +\int_{\Omega}\left[W_{i3,g}^{*}\left(x',X\right)q_3(X)+W_{i3}^{*}\left(x',X\right)q_{3,g}(X)\right]d\Omega(X) \end{aligned} \tag{5}$$

and

$$\begin{aligned} & c_{\theta\alpha}\left(x'\right)u_{\alpha,g}\left(x'\right)+\int_{\Gamma}\left[T_{\theta\alpha,g}^{*}\left(x',x\right)u_{\alpha}(x)+T_{\theta\alpha}^{*}\left(x',x\right)u_{\alpha,g}(x)\right]d\Gamma(x) \\ & +\int_{\Gamma}U_{\theta\alpha,g}^{*}\left(x',x\right)B\left[\kappa_{\alpha\beta}(1-\nu)+\nu\delta_{\alpha\beta}\kappa_{\phi\phi}\right]w_3(x)n_{\beta}(x)d\Gamma(x) \\ & +\int_{\Gamma}U_{\theta\alpha}^{*}\left(x',x\right)B\left[\kappa_{\alpha\beta}(1-\nu)+\nu\delta_{\alpha\beta}\kappa_{\phi\phi}\right] \\ & \times\left[w_{3,g}(x)n_{\beta}(x)+w_3(x)n_{\beta,g}(x)\right]d\Gamma(x) \\ & -\int_{\Omega}U_{\theta\alpha,g}^{*}\left(x',X\right)B\left[\kappa_{\alpha\beta}(1-\nu)+\nu\delta_{\alpha\beta}\kappa_{\phi\phi}\right]w_{3,\beta}(X)d\Omega(X) \\ & -\int_{\Omega}U_{\theta\alpha}^{*}\left(x',X\right)B\left[\kappa_{\alpha\beta}(1-\nu)+\nu\delta_{\alpha\beta}\kappa_{\phi\phi}\right]w_{3,\beta g}(X)d\Omega(X) \\ & =\int_{\Gamma}\left[U_{\theta\alpha,g}^{*}\left(x',x\right)t_{\alpha}(x)+U_{\theta\alpha}^{*}\left(x',x\right)t_{\alpha,g}(x)\right]d\Gamma(x) \\ & +\int_{\Omega}\left[U_{\theta\alpha,g}^{*}\left(x',X\right)q_{\alpha}(X)+U_{\theta\alpha}^{*}\left(x',X\right)q_{\alpha,g}(X)\right]d\Omega(X) \end{aligned} \tag{6}$$

where the terms $()_{,g}$ denote the derivatives with respect to $Z_g$. The same expression can be used to apply for shell structure. Expressions for the derivatives of the above terms can be found in work by Morse [25] for plate bending problems. Expressions for the derivatives of the particular solutions for the DRM are derived for the first time in this work and can be found in Appendix A.

The system of equations for the IDM-based BEM formulations is $\mathbf{H}_{,g}\mathbf{u}+\mathbf{H}\mathbf{u}_{,g} = \mathbf{G}_{,g}\mathbf{t}+\mathbf{G}\mathbf{t}_{,g}$, where the definitions of the terms $\mathbf{H}$, $\mathbf{G}$, $\mathbf{t}$, $\mathbf{u}$ are the same in Section 2.1. The terms $\mathbf{H}_{,g}$, $\mathbf{G}_{,g}$, $\mathbf{t}_{,g}$, $\mathbf{u}_{,g}$ are the derivatives of these terms. Therefore, the system of equation can be rearranged as:

$$\mathbf{AX}_{,g} = \mathbf{F}_{,g} - \mathbf{A}_{,g}\mathbf{X} \tag{7}$$

The matrices **A** and **X** can be obtained from Eq. (4). Therefore, only the right-hand side of the equation needs to be evaluated. The boundary integral equations for displacement and traction are computed in terms of the nodal coordinates of the collocation points and the field points. The derivatives of the integral equations are functions of the changes in the nodal coordinates as can be seen in Appendix A. Therefore if the change in the geometrical variable $Z_g$ does not produce a change in the nodal coordinates of both the collocation point and field point on a boundary, the corresponding entries in $\mathbf{X}_{,\mathbf{g}}$ will be zero. Consequently, the entries in $\mathbf{A}_{,\mathbf{g}}$ corresponding to this case do not need to be calculated, thereby reducing the computational cost of the IDM.

### 2.3. BEM-IDM formulations for shallow shell structures with respect to curvature $Z_\rho$

The derivatives of the shallow shell BEM formulations with respect to curvature $Z_\rho$ were derived in this work in a similar way as in the previous section. The curvatures considered in this work contain only the curvatures in the $x_1$ and $x_2$ directions such that $\kappa_{11} \neq 0$ and $\kappa_{22} \neq 0$, and $\kappa_{12} = \kappa_{21} = 0$. Hence the variable $\rho$ can only take values of $\kappa_{11}$ or $\kappa_{22}$. The derivatives of the curvature can be simplified as $\kappa_{\alpha\beta,\rho} = \delta_{\alpha\rho}\delta_{\beta\rho}$.

The derivatives of the displacement integral equation for rotations and out-of-plane displacement with respect to the curvature $Z_\rho$ is:

$$\begin{aligned}
0 = &- \int_\Omega W^*_{i3}\left(x', X\right) \kappa_{\alpha\beta,\rho} B \frac{1-\nu}{2} \\
&\times \left[u_{\alpha,\beta}(X) + u_{\beta,\alpha}(X) + \frac{2\upsilon}{1-\nu} u_{\phi,\phi}(X)\delta_{\alpha\beta}\right] d\Omega(X) \\
&- \int_\Omega W^*_{i3}\left(x', X\right) \left[\kappa_{\alpha\beta,\rho} B\left((1-\nu)\kappa_{\alpha\beta} + \nu\delta_{\alpha\beta}\kappa_{\phi\phi}\right) + \kappa_{\alpha\beta} B\left((1-\nu)\kappa_{\alpha\beta,\rho}\right.\right. \\
&\left.\left. + \nu\delta_{\alpha\beta}\kappa_{\phi\phi,\rho}\right)\right] w_3(X) d\Omega(X)
\end{aligned} \tag{8}$$

and the derivatives of the in-plane displacement integral equation is:

$$\begin{aligned}
&\int_\Gamma U^*_{\theta\alpha}\left(x', x\right) B \left[\kappa_{\alpha\beta,\rho}(1-\nu) + \nu\delta_{\alpha\beta}\kappa_{\phi\phi,\rho}\right] w_3(x) n_\beta(x) d\Gamma(x) \\
&- \int_\Gamma U^*_{\theta\alpha}\left(x', X\right) B \left[\kappa_{\alpha\beta,\rho,}(1-\nu) + \nu\delta_{\alpha\beta}\kappa_{\phi\phi,\rho}\right] w_{3,\beta}(X) d\Omega(X) \\
&= 0
\end{aligned} \tag{9}$$

The formation of the system of equations can be evaluated in a similar way as in Section 2.2:

$$\mathbf{A}\mathbf{X}_{,\rho} = \mathbf{F}_{,\rho} - \mathbf{A}_{,\rho}\mathbf{X} \tag{10}$$

A change in curvature does not result in any changes in the nodal coordinates of the source and field points, but does result in a change in the integration term with curvature-related coefficients. Since the DRM formulations do not include curvature-related coefficients, the derivatives of the DRM formulations with respect to curvature are zero and only the term relating to the curvature coefficient needs to be updated in the system of equations.

### 2.4. BEM-IDM formulations for shallow shell structures with respect to thickness $Z_h$

The derivatives of the shallow shell BEM formulations with respect to the shell thickness $Z_h$ were derived in this work in a similar way as the IDM formulation for plate thickness derivatives proposed in [21]. However, there will be an additional curvature related term in the boundary integral equations.

The derivative of the displacement integral equations for rotations and out-of-plane displacements with respect to thickness $Z_h$ are:

$$\begin{aligned}
&c_{ij}\left(x'\right) w_{j,h}(x') + \oint_\Gamma \left[P^*_{ij,h}\left(x', x\right) w_j(x) + P^*_{ij}\left(x', x\right) w_{j,h}(x)\right] d\Gamma(x) \\
&= \int_\Gamma \left[W^*_{ij,h}\left(x', x\right) p_j(x) + W^*_{ij}\left(x', x\right) p_{j,h}(x)\right] d\Gamma(x) \\
&- \int_\Omega \left[W^*_{i3,h}\left(x', X\right) B + W^*_{i3}\left(x', X\right) B_{,h}\right] \kappa_{\alpha\beta} \frac{1-\nu}{2} \\
&\times \left[u_{\alpha,\beta}(X) + u_{\beta,\alpha}(X) + \frac{2\nu}{1-\nu} u_{\phi,\phi}(X)\delta_{\alpha\beta}\right] d\Omega(X) \\
&- \int_\Omega W^*_{i3}\left(x', X\right) \kappa_{\alpha\beta} B \frac{1-\nu}{2} \\
&\times \left[u_{\alpha,\beta h}(X) + u_{\beta,\alpha h}(X) + \frac{2\nu}{1-\nu} u_{\phi,\phi h}(X)\delta_{\alpha\beta}\right] d\Omega(X) \\
&- \int_\Omega W^*_{i3}\left(x', X\right) \kappa_{\alpha\beta} B \left((1-\nu)\kappa_{\alpha\beta} + \nu\delta_{\alpha\beta}\kappa_{\phi\phi}\right) w_{3,h}(X) d\Omega(X) \\
&- \int_\Omega \left[W^*_{i3,h}\left(x', X\right) B + W^*_{i3}\left(x', X\right) B_{,h}\right] \kappa_{\alpha\beta} \left((1-\nu)\kappa_{\alpha\beta} + \nu\delta_{\alpha\beta}\kappa_{\phi\phi}\right) \\
&\times w_3(X) d\Omega(X) \\
&+ \int_\Omega W^*_{i3,h}\left(x', X\right) q_3(X) d\Omega(X)
\end{aligned} \tag{11}$$

The derivative of the in-plane displacement integral equations are:

$$\begin{aligned}
&c_{\theta\alpha}\left(x'\right) u_{\alpha,h}\left(x'\right) + \oint_\Gamma \left[T^{*(i)}_{\theta\alpha,h}\left(x', x\right) u_\alpha(x) + T^{*(i)}_{\theta\alpha}\left(x', x\right) u_{\alpha,h}(x)\right] d\Gamma(x) \\
&+ \int_\Gamma \left[U^*_{\theta\alpha,h}\left(x', x\right) B + U^*_{\theta\alpha}\left(x', x\right) B_{,h}\right] \left[\kappa_{\alpha\beta}(1-\nu) + \nu\delta_{\alpha\beta}\kappa_{\phi\phi}\right] \\
&\times w_3(x) n_\beta(x) d\Gamma(x) \\
&+ \int_\Gamma U^*_{\theta\alpha}\left(x', x\right) B \left[\kappa_{\alpha\beta}(1-\nu) + \nu\delta_{\alpha\beta}\kappa_{\phi\phi}\right] w_{,h}(x) n_\beta(x) d\Gamma(x) \\
&- \int_\Omega \left[U^*_{\theta\alpha,h}\left(x', X\right) B + U^*_{\theta\alpha}\left(x', X\right) B_{,h}\right] \left[\kappa_{\alpha\beta}(1-\nu) + \nu\delta_{\alpha\beta}\kappa_{\phi\phi}\right] \\
&\times w_{3,\beta}(X) d\Omega(X) \\
&- \int_\Omega U^*_{\theta\alpha}\left(x', X\right) B \left[\kappa_{\alpha\beta}(1-\nu) + \nu\delta_{\alpha\beta}\kappa_{\phi\phi}\right] w_{3,\beta h}(X) d\Omega(X) \\
&= \int_\Gamma \left[U^*_{\theta\alpha,h}\left(x', x\right) t_\alpha(x) + U^*_{\theta\alpha}\left(x', x\right) t_{\alpha,h}(x)\right] d\Gamma(x) \\
&+ \int_\Omega U^*_{\theta\alpha,h}\left(x', X\right) q_\alpha(X) d\Omega(X)
\end{aligned} \tag{12}$$

The formation of the system matrix is very similar to that given in the previous sections:

$$\mathbf{A}\mathbf{X}_{,\mathbf{h}} = \mathbf{F}_{,\mathbf{h}} - \mathbf{A}_{,\mathbf{h}}\mathbf{X} \tag{13}$$

### 2.5. BEM-FDM formulations for shallow shell structures

The first-order central finite difference scheme was used to estimate the first-order derivatives of a variable $S$ with respect to changes in $Z_g$, $Z_\rho$ or $Z_h$. For example, the derivative of $S$ with respect to a geometrical variable is:

$$\frac{\partial S(Z_g)}{\partial Z_g} = S_{,g} = \frac{S(Z_g + \Delta Z_g) - S(Z_g - \Delta Z_g)}{2\Delta Z_g} \tag{14}$$

where $\Delta Z_g$ is the step size. The choice of the step size has a large influence on the accuracy of the derivatives. In this work, the step size was chosen depending on the value of $Z_g$ such that $\Delta Z_g = Z_g \Delta Z'_g$, where $\Delta Z'_g$ is the normalised step size. Convergence tests were carried out to determine the optimal normalised step size. The normalised step size, $\Delta Z'_g$, used in this work ranged from 0.01 to $5 \times 10^{-4}$.

### 2.6. Evaluation of the Von Mises stress

The Von Mises stress at a boundary point can be found by:

$$\sigma_v^2 = \frac{1}{2}\left[(\sigma_{11} - \sigma_{22})^2 + \sigma_{22}^2 + \sigma_{11}^2 + 6(\sigma_{23}^2 + \sigma_{31}^2 + \sigma_{12}^2)\right] \tag{15}$$

The stress components $\sigma_{\alpha\beta}$ are defined in terms of the membrane stress resultants $N_{\alpha\beta}$, the bending stress resultants $M_{\alpha\beta}$ and the shear stress resultants $Q_\alpha$. The membrane stress resultants are assumed to be uniformly distributed throughout the thickness, while the bending stress resultants, and the shear stress resultants vary linearly through the thickness [33]. The maximum stresses occur at the top and bottom surfaces where $x_3 = \pm h/2$. Therefore, only the stresses on the top surface of the shell are of interest in this work.

$$\begin{aligned}(1+\frac{x_3}{R_\gamma})\sigma_{\alpha\beta} &= \frac{1}{h}N_{\alpha\beta}+\frac{12x_3}{h^3}M_{\alpha\beta}; \quad \begin{cases}\gamma=\beta & \alpha\neq\beta\\ \gamma\neq\beta & \alpha=\beta\end{cases}\\ (1+\frac{x_3}{R_\gamma})\sigma_{\alpha 3} &= \frac{3}{2h}\left[1-\left(\frac{2x_3}{h}\right)^2\right]Q_\alpha; \quad \gamma\neq\alpha\end{aligned} \tag{16}$$

The direct method [2] was used to evaluate the stress resultants in terms of the strain and boundary tractions. A detailed derivation can be found in [32], and only a brief introduction is presented here. The local bending stress resultants are defined as:

$$\begin{aligned}\hat{M}_{11} &= \hat{p}_1\\ \hat{M}_{12} &= \hat{p}_2\\ \hat{M}_{22} &= \nu\hat{M}_{11}+D(1+\nu^2)\hat{\chi}_{22}+\frac{q\nu}{\lambda^2}\end{aligned} \tag{17}$$

where $\hat{p}_1$ and $\hat{p}_2$ are the local normal and tangential components of traction and are defined as $\hat{p}_1 = n_1p_1+n_2p_2$ and $\hat{p}_2 = -n_2p_1+n_1p_2$, where $p_1$ and $p_2$ are the global boundary traction derived from the boundary integral equations in Eq. (4). The local tangential strain $\hat{\chi}_{22}$ is:

$$\hat{\chi}_{22} = \frac{e_{2\alpha}}{J(\zeta)}\sum\left(w_\alpha\frac{dN(\zeta)}{d\zeta}\right) \tag{18}$$

where $J(\zeta)$ is the Jacobian, $N(\zeta)$ is the two dimensional quadratic shape functions and $e_{\alpha\beta}$ is the rotation matrix where

$$e_{\alpha\beta} = \begin{bmatrix} n_1 & n_2\\ -n_2 & n_1\end{bmatrix} \tag{19}$$

Once the local bending stress resultants are obtained, the global bending stress resultants can be evaluated using the rotation matrix as:

$$M_{\alpha\beta} = e_{\psi\alpha}e_{\phi\beta}\hat{M}_{\psi\phi} \tag{20}$$

The membrane stress resultants are defined such that:

$$\begin{aligned}\hat{N}_{1\alpha} &= \hat{t}_\alpha\\ \hat{N}_{22} &= \frac{1}{1-\nu}\left[\frac{Eh}{1+\nu}\hat{\varepsilon}_{22}+\nu\hat{t}_1\right]+B(\nu\kappa_{11}+\kappa_{22})\hat{w}_3\end{aligned} \tag{21}$$

where

$$\hat{\varepsilon}_{22} = \frac{e_{2\alpha}}{J(\zeta)}\sum\left(u_\alpha\frac{dN(\zeta)}{d\zeta}\right) \tag{22}$$

The local normal and tangential traction components can be found in a similar way such that $\hat{t}_1 = n_1t_1+n_2t_2$ and $\hat{t}_2 = -n_2t_1+n_1t_2$, where $t_1$ and $t_2$ are the global membrane tractions. The global membrane stress resultant can be found by using the rotation matrix:

$$N_{\alpha\beta} = e_{\psi\alpha}e_{\phi\beta}\hat{N}_{\psi\phi} \tag{23}$$

The shear stress resultant can be evaluated as:

$$\begin{aligned}\hat{Q}_1 &= p_3\\ \hat{Q}_2 &= D\frac{1-\nu}{2}\lambda^2(u\hat{v}_2+\hat{w}_{3,2})\end{aligned} \tag{24}$$

where $\hat{w}_2 = -n_2w_1+n_1w_2$ and

$$\hat{w}_{3,2} = \frac{1}{J(\zeta)}\sum\left(\hat{w}_3\frac{dN(\zeta)}{d\zeta}\right) \tag{25}$$

The global shear stress resultant at a boundary point is therefore

$$\begin{aligned}Q_1 &= \hat{Q}_1n_1-\hat{Q}_2n_2\\ Q_2 &= \hat{Q}_1n_2+\hat{Q}_2n_1\end{aligned} \tag{26}$$

### 2.7. Derivatives of the boundary stress resultants

In this section, the derivatives of the boundary stress resultants from the previous section are presented here with respect to geometrical variables, curvature, and thickness. The derivatives of the bending stress resultants $M_{\alpha\beta}$ and shear stress resultants $Q_\alpha$ for plates have been derived in previous literature with respect to geometrical variables [21,34,35] and with respect to thickness [21]. These same equations can be applied to shells as well. A detailed description of the formulations are presented in Appendix C. However, the derivatives of the membrane stress resultants $N_{\alpha\beta}$ will be different for shells compared to plates. The derivatives of the membrane stress resultants $N_{\alpha\beta}$ for shells are presented for the first time in this work.

The derivatives of the membrane stress resultants $N_{\alpha\beta}$ in Eq. (21) with respect to a geometrical variable $Z_g$ can be evaluated as:

$$\begin{aligned}\hat{N}_{1\alpha,g} &= \hat{t}_{\alpha,g}\\ \hat{N}_{22,g} &= \frac{1}{1-\nu}\left[\nu\hat{t}_{1,g}+\frac{Eh}{1+\upsilon}\hat{\varepsilon}_{22,g}\right]+B\left(\nu\kappa_{11}+\kappa_{22}\right)\hat{w}_{3,g}\end{aligned} \tag{27}$$

where

$$\begin{aligned}\hat{\varepsilon}_{22,g} = \frac{1}{J(\zeta)}\Bigg[&e_{2\alpha,g}\sum\left(\hat{u}_\alpha\left(\frac{dN(\zeta)}{d\zeta}\right)\right)-J_{,g}(\zeta)\hat{\varepsilon}_{22}\\ &+e_{2\alpha}\sum\left(\hat{u}_{\alpha,g}\left(\frac{dN(\zeta)}{d\zeta}\right)\right)\Bigg]\end{aligned} \tag{28}$$

The corresponding IDM formulations for stress couples $\sigma_{\alpha\beta}$ in Eq. (16) with respect to $Z_g$ at the top surface $x_3 = h/2$ can be derived as:

$$\begin{aligned}\sigma_{\alpha\beta,g} &= \left(\frac{1}{h}N_{\alpha\beta,g}+\frac{b}{h^2}M_{\alpha\beta,g}\right)/\left(1+\frac{h}{2}\kappa_\gamma\right)\\ \sigma_{\alpha 3,g} &= \frac{3}{2h}Q_{\alpha,g}/\left(1+\frac{h}{2}\kappa_\gamma\right)\end{aligned} \tag{29}$$

The derivatives of the membrane stress resultant in Eq. (21) with respect to a curvature $Z_\rho$ can be evaluated as:

$$\begin{aligned}\hat{N}_{1\alpha,\rho} &= \hat{t}_{\alpha,\rho}\\ \hat{N}_{22,\rho} &= \frac{1}{1-\upsilon}\left[\upsilon\hat{t}_{1,\rho}\frac{Eh}{1+\upsilon}\hat{\varepsilon}_{22,\rho}\right]+B\left(\nu\kappa_{11,\rho}+\kappa_{22,\rho},\right)\hat{w}_3\\ &\quad+B\left(\nu\kappa_{11}+\kappa_{22}\right)\hat{w}_{3,\rho}\end{aligned} \tag{30}$$

where

$$\hat{\varepsilon}_{22,\rho} = \frac{e_{2\alpha}}{J(\zeta)}\sum_{i=1}^{M}\left(\hat{u}_{\alpha,\rho}\left(\frac{dN(\zeta)}{d\zeta}\right)\right) \tag{31}$$

The corresponding IDM formulations for stress couples $\sigma_{\alpha\beta}$ in Eq. (16) with respect to $Z_\rho$ at the top surface can be derived as:

$$\begin{aligned}\sigma_{\alpha\beta,\rho} &= \left(\frac{1}{h}N_{\alpha\beta,\rho}+\frac{6}{h^2}M_{\alpha\beta,\rho}\right)/\left(1+\frac{h}{2}\kappa_\gamma\right)-\sigma_{\alpha\beta}h/(2+h\kappa_\gamma)\\ \sigma_{\alpha 3,\rho} &= \frac{3}{2h}Q_{\alpha,\rho}/\left(1+\frac{h}{2}\kappa_\gamma\right)-\sigma_{\alpha 3}h/(2+h\kappa_\gamma)\end{aligned} \tag{32}$$

The derivatives of the membrane stress resultants in Eq. (21) with respect to thickness $Z_h$ can be evaluated as:

$$\begin{aligned}\hat{N}_{1\alpha,h} &= \hat{t}_{\alpha,h}\\ \hat{N}_{22,h} &= \frac{1}{1-\upsilon}\left[\nu\hat{t}_{1,h}+\frac{Eh}{1+\upsilon}\hat{\varepsilon}_{22,h}+\frac{E}{1+\upsilon}\hat{\varepsilon}_{22}\right]\\ &\quad+B\left(\nu\kappa_{11}+\kappa_{22}\right)\hat{w}_{3,h}+B_{,h}\left(\upsilon\kappa_{11}+\kappa_{22}\right)\hat{w}_3\end{aligned} \tag{33}$$

where

$$\hat{\varepsilon}_{22,h} = \frac{e_{2\alpha}}{J(\zeta)}\sum_{i=1}^{M}\left(\hat{u}_{\alpha,h}\left(\frac{dN(\zeta)}{d\zeta}\right)\right)$$

The corresponding IDM formulations for stress couples $\sigma_{\alpha\beta}$ in Eq. (16) with respect to $Z_h$ at the top surface can be derived as:

$$\begin{aligned}\sigma_{\alpha\beta,h} &= \left(\frac{6}{h^2}M_{\alpha\beta,h}+\frac{1}{h}N_{11,h}-\frac{12}{h^3}M_{\alpha\beta}-\frac{1}{h^2}N_{\alpha\beta}\right)/\left(1+\frac{h}{2}\kappa_\gamma\right)\\ &\quad-\sigma_{\alpha\beta}\kappa_\gamma/(2+h\kappa_\gamma)\\ \sigma_{\alpha 3,h} &= \frac{3}{2}Q_{\alpha,h}/(1+\frac{h}{2}\kappa_\gamma)-\sigma_{\alpha 3}/h-\sigma_{\alpha 3}\kappa_\gamma/(2+h\kappa_\gamma)\end{aligned} \tag{34}$$

where $\kappa_\gamma = 1/R_\gamma$. The detailed IDM formulations for $M_{\alpha\beta,g}$, $M_{\alpha\beta,\rho}$, $M_{\alpha\beta,h}$ and $Q_{\alpha,g}$, $Q_{\alpha,\rho}$, and $Q_{\alpha,h}$ can be found in Appendix C.

The IDM formulations for the Von Mises stress can therefore be derived as:

$$\sigma_{v,m} = \frac{1}{2\sigma_v}\left[(\sigma_{11}-\sigma_{22})(\sigma_{11,m}-\sigma_{22,m}) + \sigma_{22}\sigma_{22,m} + \sigma_{11}\sigma_{11,m} + 12(\sigma_{23}\sigma_{23,m} + \sigma_{31}\sigma_{31,m} + \sigma_{12}\sigma_{12,m})\right] \tag{35}$$

where the subscript "$,m$" indicates a derivative with respect to a geometrical variable, curvature, or thickness.

### 2.8. The First-Order Reliability Method (FORM)

The purpose of this section is to provide a brief introduction to the First-Order Reliability Method (FORM). A more detailed introduction can be found in [36].

The Most-Probable Point (MPP) approach was used in this work with the FORM to evaluate the reliability index. Typically, the MPP is located through the use of an iterative algorithm, details of which can be found in [37,38].

In structural reliability analysis, the boundary between the safe domain and the failure domain is defined by a Limit State Function (LSF):

$$g(\mathbf{Z}) = G_0 - G(\mathbf{Z}) \tag{36}$$

where $G_0$ is the structure's resistance to loading e.g. fracture toughness, yield strength, or maximum allowable displacement. $\mathbf{Z}$ is a vector that contains the values of the design variables that could affect $g(\mathbf{Z})$. The failure boundary is therefore $g(\mathbf{Z}) = 0$. The failure domain is defined as $g(\mathbf{Z}) < 0$, while the safe domain is defined as $g(\mathbf{Z}) > 0$

Reliability can be determined by evaluating the following integral:

$$P_R = 1 - P_F = P\{g(\mathbf{Z}) > 0\} = \int_{g(\mathbf{Z})>0} f_Z(\mathbf{Z}) dZ \tag{37}$$

where $f_Z(\mathbf{Z})$ is the joint Probability Density Function (PDF) of $\mathbf{Z}$, $P_R$ is the reliability, and $P_F$ is the failure probability. This equation involves the integration over the safe domain $g(\mathbf{Z}) > 0$. This could be difficult since the vector of design variables could be multidimensional. Therefore, a commonly used method, the FORM, was applied to approximate the LSF using the first-order Taylor expansion.

The FORM involves transferring the variable from $\mathbf{Z}$-space to the standard normal $\mathbf{U}$-space, where variables in $\mathbf{Z}$ can be expressed in terms of $\mathbf{U}$, the means and the standard deviations of $\mathbf{Z}$. Eq. (37) can be transferred to $\mathbf{U}$-space as:

$$P_R = 1 - P_F = P\{g(\mathbf{U}) > 0\} = \int_{g(\mathbf{U})>0} f_U(\mathbf{U}) dU \tag{38}$$

The FORM relies on approximating the LSF using a first-order Taylor expansion:

$$g(\mathbf{U}) \approx g(\mathbf{u}^*) + \nabla g(\mathbf{u}^*)(\mathbf{U} - \mathbf{u}^*) \tag{39}$$

where $u^*$ is the expansion point. The gradient of $g(\mathbf{U})$ is defined as:

$$\nabla g(\mathbf{u}^*) = \left(\frac{\partial g(\mathbf{U})}{\partial U_1}, \frac{\partial g(\mathbf{U})}{\partial U_2}, \ldots, \frac{\partial g(\mathbf{U})}{\partial U_n}\right)\Bigg|_{\mathbf{u}^*} \tag{40}$$

Ideally, the integration function should be expanded at a point that has the highest probability density and highest contribution to the integration. This point is the MPP and is located somewhere along the boundary $g(\mathbf{U}) = 0$. The reliability index is the distance between the MPP to the origin of the $\mathbf{U}$-space and is denoted as $\beta$. Reliability and probability of failure are related to $\beta$:

$$P_R = 1 - P_F = 1 - \Phi(-\beta) = \Phi(\beta) \tag{41}$$

where $\Phi(\beta)$ is the Cumulative Distribution Function (CDF) of the standard normal distribution.

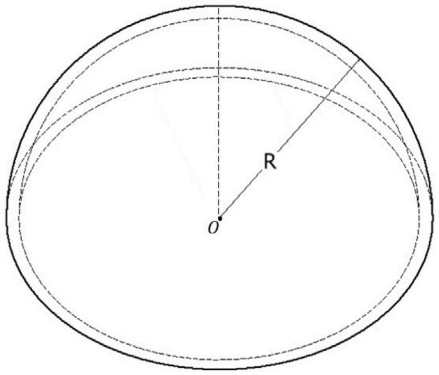


**Fig. 2.** Hemispherical shell under normal pressure with radius of curvature $R$.

**Table 1**
Results of the derivatives of the centre deflection with respect to the curvature $w_{3,R}$ obtained from the analytical solution, IDM and FDM. The derivatives are given in magnitude of $10^{-4}$. Percentage differences (%) between the IDM and the analytical solution.

| h/R | R | h | Analytical | IDM | FDM | % diff |
|---|---|---|---|---|---|---|
| 1/100 | 5000 | 50 | 0.450 | 0.454 | 0.454 | 0.980 |
| 1/200 | 5000 | 25 | 0.900 | 0.901 | 0.901 | 0.147 |
| 1/500 | 12 500 | 25 | 2.25 | 2.25 | 2.25 | 0.169 |
| 1/1000 | 25 000 | 25 | 4.50 | 4.51 | 4.51 | 0.241 |
| 1/5000 | 125 000 | 25 | 22.5 | 22.6 | 22.6 | 0.407 |

## 3. Analytical validation of the BEM-IDM formulation

It is necessary to validate the accuracy of the derived BEM-IDM formulations when calculating sensitivities. A comparison is first made between the results from the IDM and the analytical solution for a hemispherical shell under normal pressure in [39]. The hemispherical shell is simply supported around the edge of its circular base, and it has a radius of curvature $R$ and thickness $h$. It is subjected to uniform pressure $p = 10$ kN/m$^2$ acting in the out-of-plane direction. The shell has a Young's modulus of $E = 2.0 \times 10^7$ kN/m$^2$ and Poisson's ratio $\nu = 0.1$. The curvature of the shell is calculated as $\kappa_{11} = \kappa_{22} = 1/R$. The geometry is shown in Fig. 2.

The out-of-plane displacement at the center of the shell is given by

$$w_3 = (1-\nu)pR^2/2Eh \tag{42}$$

The derivative of the out-of-plane displacement at the shell centre with respect to the radius of the curvature $R$ and with respect to the thickness $h$ is:

$$w_{3,R} = (1-\nu)pR/Eh; \qquad w_{3,h} = -(1-\nu)pR^2/Eh^2 \tag{43}$$

The BEM model consists of 48 quadratic elements on the boundaries and 49 DRM points which are distributed evenly in the domain. The out-of-plane displacement obtained from BEM was compared to that obtained by the analytical solution. The derivative was calculated from both FDM and IDM at different values of $h/R$. The normalised step size used for the FDM was $\Delta Z'_g = 0.01$. The percentage difference between the analytical solution and the IDM/FDM solutions were then calculated. The results for $w_{3,R}$ and $w_{3,h}$ are given in Tables 1 and 2, respectively.

As seen in Tables 1 and 2, the difference between the IDM and the analytical solution is less than 1% for $w_{3,R}$ and less than 3% for $w_{3,h}$. There are only minor differences between the results obtained from the FDM and the IDM, which indicates that the IDM provides a similar level of accuracy to the FDM. However, to determine the optimal step size for FDM, a convergence test must be performed, whereas the accuracy of IDM does not require a step size, making it a more robust alternative to the FDM. In conclusion, the IDM formulations was

**Table 2**
Results of the derivatives of the centre deflection with respect to the thickness $w_{3,h}$ obtained from the analytical solution, IDM and FDM. Percentage differences (%) between the IDM and the analytical solution.

| h/R | R | h | Analytical | IDM | FDM | % diff |
|---|---|---|---|---|---|---|
| 1/100 | 5000 | 50 | −2.25E−03 | −2.19E−03 | −2.19E−03 | 2.61 |
| 1/200 | 5000 | 25 | −9.00E−03 | −8.90E−03 | −8.90E−03 | 1.09 |
| 1/500 | 12 500 | 25 | −5.63E−02 | −5.62E−02 | −5.62E−02 | 0.01 |
| 1/1000 | 25 000 | 25 | −2.25E−01 | −2.26E−01 | −2.26E−01 | 0.24 |
| 1/5000 | 125 000 | 25 | −5.63E+00 | −5.65E+00 | −5.65E+00 | 0.46 |

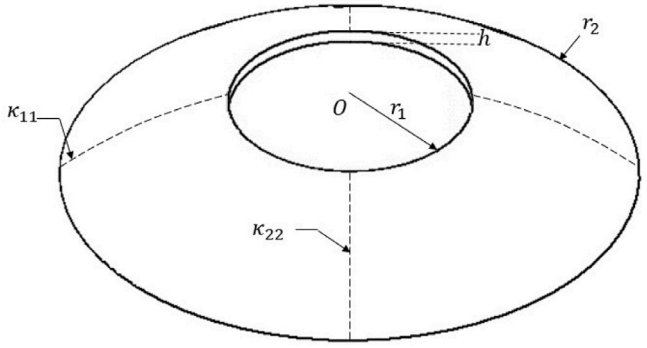


**Fig. 3.** Circular shallow spherical shell with a hole in the centre. The shell is subjected under a uniform pressure load acting against the curvature (downward). The shell contains an inner radius of $r_1$ and an outer radius of $r_2$, the thickness of the shell $h$. The curvatures in x and y direction are $\kappa_{11} = \kappa_{22} = \kappa$.

successfully validated against the analytical solution and demonstrated a good level of accuracy and robustness.

## 4. Numerical examples

A numerical example featuring a clamped circular shallow spherical shell was used to demonstrate the use of the IDM formulation with the FORM. Various geometrical parameters and material properties were treated as random variables. The geometry of the shell is shown in Fig. 3.

The outer boundary of the shell is clamped, and the shell is subjected to a uniform pressure load. The shell is composed of Aluminium 6061-T6 with Young's modulus of $E = 68.9$ GPa, Poisson's ratio of $\nu = 0.33$ and yield strength $\sigma_y = 276$ MPa [40]. The shell has a thickness $h$, and the curvature in the x and y-direction is denoted as $\kappa_{11}$, $\kappa_{22}$, respectively. In this work the curvatures are assumed to be equal, that is $\kappa_{11} = \kappa_{22} = \kappa$. The geometrical variables consisting of the inner radius $r_1$ and outer radius $r_2$ of the boundaries of the shell, the thickness of the shell $h$, along with the Poisson's ratio $\nu$, curvature $\kappa$ and loading conditions $p$ are treated as random variables in the FORM. Details of these random variables can be found in Table 3. In the curvature, the Coefficient Of Variation (COV) is considered to be a variable for representing different levels of manufacturing uncertainty.

The BEM model of the shell consists of 64 quadratic elements. 32 elements were used to discretise the inner boundary and 32 elements for the outer boundary. 64 DRM points were evenly distributed in the domain.

### 4.1. Reliability analysis

The failure condition of the shell is defined such that the maximum Von Mises stress found in the shell does not exceed the yield strength of the material. The Limit State Function (LSF) in this case is:

$$g(\mathbf{Z}) = \sigma_y - \sigma_v^{max}(\mathbf{X}) \tag{44}$$

where $\sigma_y$ is the yield strength and $\sigma_v^{max}$ is the maximum Von Mises stress. The vector $\mathbf{Z}$ contains the design variables that can influence

**Table 3**
The design variables used in the reliability analyses.

| $Z_i$ | $X_i$ | Parameter | Description | Distribution | Mean | COV |
|---|---|---|---|---|---|---|
| $Z_1$ | $X_1$ | $r_1$ | Inner radius | Normal | 0.5 m | 0.1 |
| $Z_2$ | $X_2$ | $r_2$ | Outer radius | Normal | 5 m | 0.1 |
| $Z_3$ | $X_3$ | $\kappa$ | Curvature in x direction | Normal | 0.005 $m^{-1}$ | $COV_\kappa$ |
| $Z_4$ | $X_4$ | $h$ | Shell thickness | Normal | 0.05 m | 0.05 |
| $Z_5$ | $X_5$ | $\nu$ | Poisson's ratio | Normal | 0.3 | 0.05 |
| $Z_6$ | $X_6$ | $p$ | Domain pressure | Normal | 0.025 MPa | 0.2 |

**Table 4**
CPU time required for the FORM, with either the IDM or the FDM.

| Method | CPU time (s) per derivative |
|---|---|
| FDM | 2.41 |
| IDM | 1.55 |

the value of $g$ where $\mathbf{Z} = (r_1, r_2, \kappa, h, \nu, p, \sigma_y)$ and $\mathbf{X}$ consist of the design variables in $\mathbf{Z}$ without the yield strength $\mathbf{X} = (r_1, r_2, \kappa, h, \nu, p)$. In the FORM, the sensitivity of $g(\mathbf{Z})$ with respect to the design parameter $Z_i$ is needed. The IDM involves calculating the direct derivatives of boundary integral equations defined in terms of the source point and the field point. In order to conduct the IDM, it is necessary to estimate the derivatives of the nodal coordinates of the collocation points. The geometrical variables $Z_1 - Z_4$ were evaluated analytically using the BEM-IDM to determine the sensitivities. For the non-geometrical variables $Z_5 - Z_6$, the sensitivities were determined by using the DBEM-FDM with a step size of $\Delta Z_g' = 5\times10^{-4}$. A range of possible $COV_\kappa$ values for curvature were tested from 0.02 to 0.2.

The results of the influence of the $COV_\kappa$ on the overall structural reliability are shown in Fig. 4. The reliability of the structure decreased as the $COV_\kappa$ increased, which indicated that higher uncertainties result in a higher probability of failure. In comparison to the FDM-FORM, there are only minor differences between the IDM-FORM and the FDM-FORM with a maximum difference of 0.11% at $COV_\kappa = 0.2$. The IDM-FORM is more computationally efficient than the FDM-FORM, as seen by the CPU times shown in Table 4 for evaluating one derivative for a single parameter. In terms of the CPU time required by the FORM, the IDM is 35% faster than the FDM. Although this represents a reduction of only 0.86 s, this reduction can prove significant when large amount of derivatives are needed, such as in gradient-based optimisation. This improvement in efficiency offered by the IDM is compounded by the fact that the FDM requires the use of a step-size, while the IDM does not. These results indicate that the novel IDM developed in this work is a significantly more efficient alternative to the FDM when calculating sensitivities.

### 4.2. Sensitivity analysis

Reliability analysis provides a means of assessing structural reliability and safety, the results of which can be used for sensitivity analyses to identify the most important design parameters for improving safety. As the number of random variables associated with the response of a structure increases, it becomes increasingly difficult to control all of the variables in order to improve the reliability. Instead, only the variables that are the most important need to be identified and managed. In order to quantify the influence of uncertainty in parameters on overall reliability, reliability sensitivity analysis are usually conducted to analyse the effect of individual parameters on the failure probability.

A sensitivity factor is defined as the rate of change in the probability of failure with respect to a distribution parameter ($\mu$ or $\sigma$) of a variable. The sensitivity factors in this work were evaluated at the design point (i.e. MPP) for different values of COV of the curvature $COV_\kappa$.

For the variables with a normal distribution, the sensitivity factor for the mean or standard deviation can be derived as [36]:

$$S_{\mu_i} = \frac{\partial P_f}{\partial \mu_i} = \phi(-\beta)\frac{u_i^*}{\beta\sigma_i}; \qquad S_{\sigma_i} = \frac{\partial P_f}{\partial \sigma_i} = \phi(-\beta)\frac{(u_i^*)^2}{\beta\sigma_i} \tag{45}$$

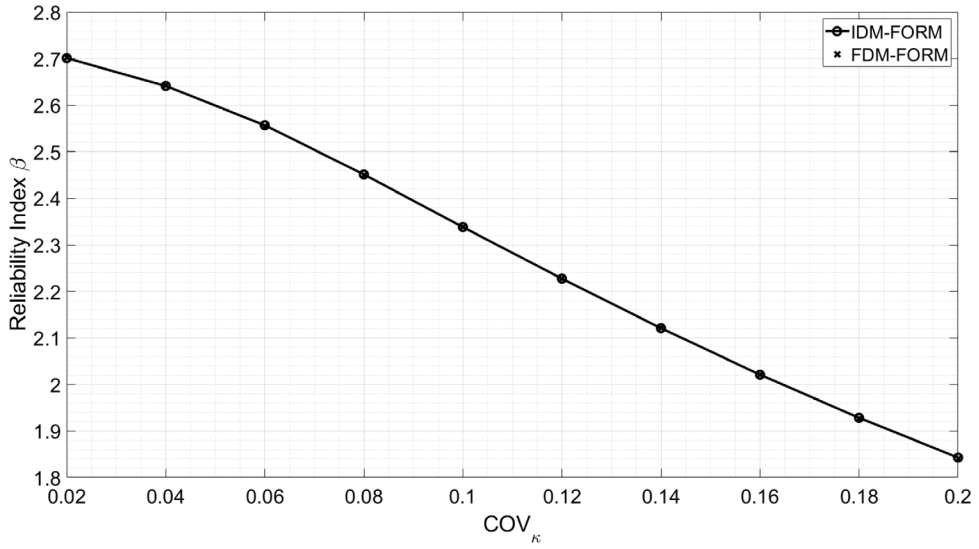


**Fig. 4.** Effect of the uncertainties (COV) in the curvature on the Reliability index for IDM and FDM compare to the results obtained from MCS.

**Table 5**
The sensitivity factors obtained from the reliability analysis for $COV_\kappa = 0.1$. The table gives both the sensitivity factor and the normalised sensitivity factors.

| Sensitivity | $S_{\mu_i}$ | $\widetilde{S}_{\mu_i}$ | Sensitivity | $S_{\sigma_i}$ | $\widetilde{S}_{\sigma_i}$ |
|---|---|---|---|---|---|
| $\partial P_f/\partial \mu_{r_1}$ | −0.018 | −0.93 | $\partial P_f/\partial \sigma_{r_1}$ | 0.0015 | 0.0076 |
| $\partial P_f/\partial \mu_{r_2}$ | 0.011 | 5.49 | $\partial P_f/\partial \sigma_{r_2}$ | 0.0051 | 0.26 |
| $\partial P_f/\partial \mu_\kappa$ | −25.65 | −13.24 | $\partial P_f/\partial \sigma_\kappa$ | 29.67 | 1.53 |
| $\partial P_f/\partial \mu_h$ | −3.38 | −17.45 | $\partial P_f/\partial \sigma_h$ | 2.58 | 0.67 |
| $\partial P_f/\partial \mu_\nu$ | 0.077 | 2.38 | $\partial P_f/\partial \sigma_\nu$ | 0.0080 | 0.012 |
| $\partial P_f/\partial \mu_p$ | 4.03 | 10.40 | $\partial P_f/\partial \sigma_p$ | 7.32 | 3.78 |

where $\beta$ is the reliability index evaluated at the MPP and $\phi(-\beta)$ is the probability density function of a standard normal distribution at $-\beta$. $u_i^*$ is the corresponding U-space value of the MPP.

The sensitivity factors obtained from Eq. (45), $S_{\mu_i}$ and $S_{\sigma_i}$ are not directly comparable with each other since they are have different units. Therefore, a dimensionless process was applied to make the sensitivity factors unit-independent [41] such that:

$$\widetilde{S}_{\mu_i} = \frac{\mu_i}{P_f}\frac{\partial P_f}{\partial \mu_i}; \qquad \widetilde{S}_{\sigma_i} = \frac{\sigma_i}{P_f}\frac{\partial P_f}{\partial \sigma_i} \tag{46}$$

where $\widetilde{S}_{\mu_i}$ and $\widetilde{S}_{\sigma_i}$ represent the sensitivity of failure probability with respect to the mean and standard deviation of the distribution, respectively. The results of the sensitivity factors evaluated at the MPP at $COV_\kappa = 0.1$ are given in Table 5.

It can be seen from Table 5 that the sign of the sensitivity factor for the outer radius mean, Poisson's ratio, and pressure load, is positive. This indicates that the probability of failure will increase as the mean value of these variables increases. The opposite is true for sensitivity factors with negative signs. This is intuitive, for example, as the value of curvature decreases, the structure more closely resembles a flat plate structure, which has less resistance to downward pressure. Also, a thicker shell will be able to withstand larger pressure forces. All the sensitivity factors for the standard deviation are of positive sign, which is intuitive and consistent with the expectation that increasing uncertainties in the variables will lead to a greater probability of failure.

Sensitivity analysis can be a helpful tool in the design process. However, if there is a large number of variables involved, it can be difficult to determine the variables that have the most significant effect on reliability. The percentage importance of each of the random variables can be calculated as [42]:

$$\lambda_{\mu_i} = \frac{|\widetilde{S}_{\mu_i}|}{\sum|\widetilde{S}_{\mu_i}|} \times 100\%; \qquad \lambda_{\sigma_i} = \frac{|\widetilde{S}_{\sigma_i}|}{\sum|\widetilde{S}_{\sigma_i}|} \times 100\%; \tag{47}$$

where $\lambda_{\mu_i}$ and $\lambda_{\sigma_i}$ represents the percentage contribution of each distribution parameter to the total sensitivity. The percentage sensitivity factors for different variables and for different values of $COV_\kappa$ are shown in Figs. 5 and 6 for the means and standard deviations, respectively.

Based on the results, it can be seen that the mean and standard deviation of both the inner radius $r_1$ and Poisson's ratio $\nu$ have a much smaller impact on the sensitivity than the other parameters. This contrasts with the other geometric variables, the failure probability is much more sensitive to variations in curvature $\kappa$ and thickness $h$. Out of all the parameters, the standard deviation of the applied uniform pressure $\sigma_p$ has the largest impact on the probability of failure. However, as $COV_\kappa$ increases, the standard deviation of the curvature $\sigma_\kappa$ reaches a similar level of impact.

In summary, these results indicate that to improve the reliability of the shallow shell structure seen in Fig. 3, more consideration should be given to the curvature and thickness, as they have a significant impact on failure probability and are easier to control compared to non-geometrical parameters, such as the applied pressure. Moreover, more effort should be made to quantify the uncertainties in the applied pressure load, since the standard deviation in the pressure load has a significant impact on the failure probability.

## 5. Optimisation

The IDM formulation was used in the previous two examples to evaluate the response sensitivities of a structure with respect to design parameters. The IDM formulations were first validated through an analytical example, then a more complicated example was analysed to identify the most influential design parameters. To demonstrate further application of the IDM formulations for practical purposes, two optimisation examples were investigated involving shape optimisation using the novel IDM methodology developed in this work. The first optimisation example involved the shape optimisation of the circular shell structure analysed in Section 4. The second optimisation example involved optimising the shape of an aircraft fuselage structure; a significantly more complex geometry with many more design parameters than the first example.

Optimisation during the design stage enables engineers to maximise/minimise a performance function subjected to constraints or

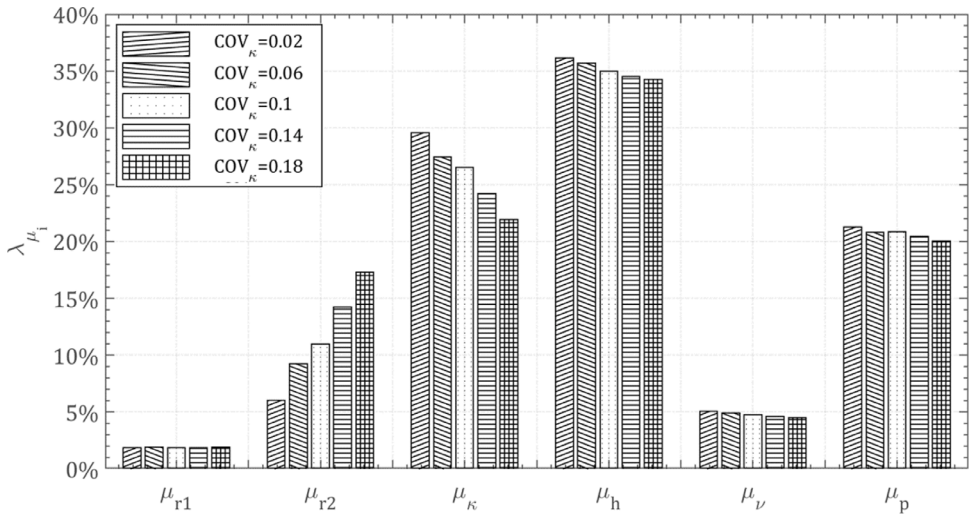


**Fig. 5.** Percentage influence of the sensitivity factors of mean of the variables with varying COV in curvature.

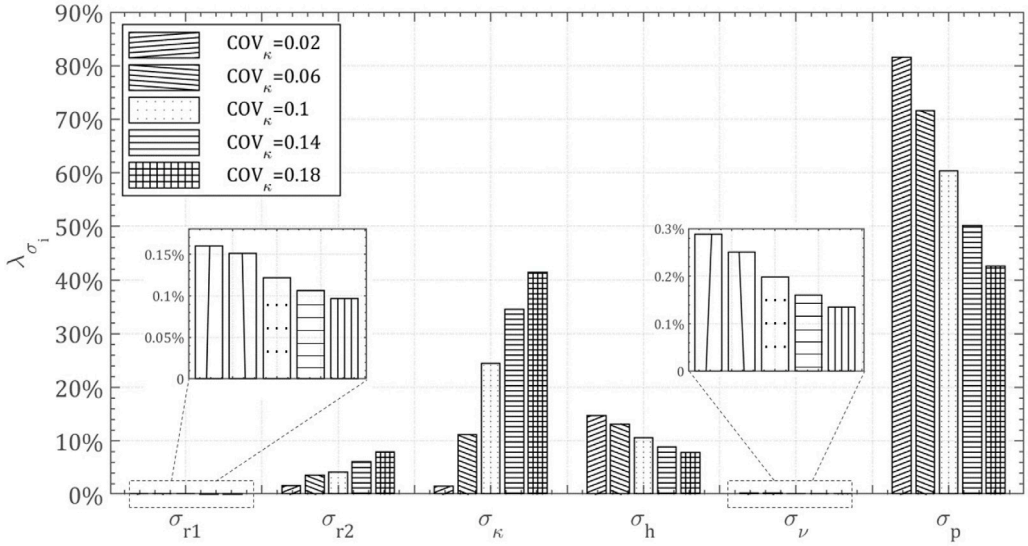


**Fig. 6.** Percentage influence of the sensitivity factors of standard deviation of the variables with varying COV in curvature.

requirements of the structure. Since the sensitivities are already calculated in the FORM via the method introduced in the previous sections in cooperation with the BEM, gradient-based design optimisation methods were used. The optimisation was conducted in MATLAB using the nonlinear multi-variable function solver 'fmincon'.

### 5.1. Numerical example 1: Circular shallow spherical shell

The first example involves the optimisation of a circular shell with a centre hole shown in the previous Section 4.2. The shape of the shell is optimised such that its mass is minimised subjected to the requirement that the maximum Von Mises stress cannot exceed a certain limit. According to the sensitivity analysis results shown in Section 4.2, the outer radius $r_2$, curvature $\kappa$ and the thickness $h$ have the most impact on the maximum Von Mises stress in the structure. Therefore, only $\mathbf{d} = [r_2, \kappa, h]$ were considered as design parameters during the optimisation. Other parameters were fixed at their mean value. The optimisation problem is therefore defined as:

$$\begin{aligned} &\text{Minimise:} && Mass(\mathbf{d}) \\ &\text{Subject to:} && \mathbf{d}^L \le \mathbf{d} \le \mathbf{d}^U, \quad \mathbf{d} \in \mathbf{R}^3 \end{aligned} \tag{48}$$

$$\sigma_v^{max} \le \sigma_Y / S$$

where $\sigma_v^{max}$ is the maximum Von Mises stress in the structure, $\sigma_Y$ is the yield strength and $S$ is the safety factor with a value of 1.5. The initial design is $\mathbf{d}_0 = [5, 0.05, 0.5]$ with the lower bound $\mathbf{d}^L = [4.5, 0.001, 0.01]$ and upper bound $\mathbf{d}^U = [5.5, 0.01, 0.1]$. The optimisation procedure is considered to have converged when the change in $Mass(\mathbf{d})$ is less than 0.01% and $\sigma_v^{max}$ is below or equal to $\sigma_Y$ within 0.01% error. Several materials, Aluminium 6061-T6, 2024-T4, 7075-T6, and 7075-T7, were tested to investigate the effect of yield strength on the optimisation results. The material properties of these materials are summarised in Table 6 and the mass can be calculated using the design variables $\mathbf{d}$ with the corresponding density. The volume of the initial design is 3.889 m$^3$. It is expected that when a material with higher yield strength is used, the mass of the optimised design will be lighter.

The optimisation results for each of these materials are given in Table 7 and the convergence history is shown in Fig. 7. The shape of the structure is shown in Fig. 7 at three different iterations. It can be seen that the optimisation successfully decreases the volume of the structure compared to the initial design. The results show that when a material with a higher yield strength was used, such as Aluminium 7075-T6, a lighter mass can be achieved. This matches the expected outcome discussed earlier.

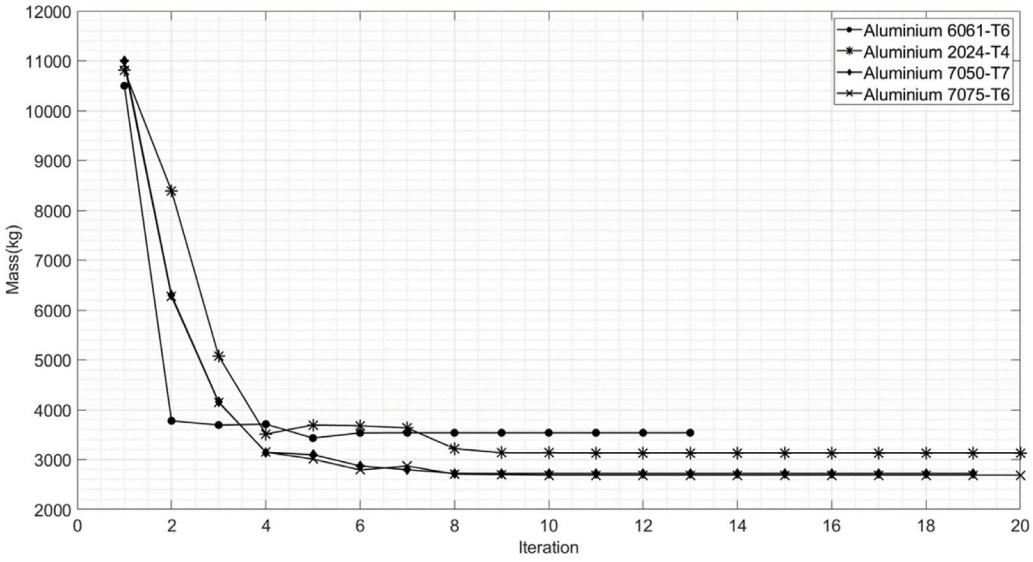


**Fig. 7.** Optimisation history from the IDM-based BEM with multiple Aluminium alloys. Three examples of shape-changing in the optimisation are presented for Aluminium 2024-T4.

**Table 6**
Material properties of different Aluminium alloys. The Young's modulus $E$, Poisson's ratio $\nu$, yield strength $\sigma_Y$ and density $\rho$ are given [40].

| Material | $E$ [GPa] | $\nu$ | $\sigma_Y$ [MPa] | $\rho$ [kg m$^{-3}$] |
|---|---|---|---|---|
| Aluminium 6061-T6 | 68.9 | 0.33 | 276 | 2700 |
| Aluminium 2024-T4 | 73.1 | 0.33 | 324 | 2780 |
| Aluminium 7050-T7 | 71.7 | 0.33 | 469 | 2830 |
| Aluminium 7075-T6 | 71.7 | 0.33 | 503 | 2810 |

### 5.2. Numerical example 2: Shell structure with a window

The aim of this second example is to demonstrate the application of the BEM-IDM to Reliability-Based Design Optimisation (RBDO). RBDO involves optimising a structure for a specific level of reliability and accounts for uncertainties in the design parameters. RBDO has been widely studied in the literature [20,21,43,44]. Common approaches for performing RBDO are the Reliability Index Approach (RIA) and the Performance Measurement Approach (PMA). The PMA was used in this work due to its fast convergence and superior stability [44].

The simply supported shell structure with a window section is shown in Fig. 8. The structure is composed of Aluminium 6061-T6, and is subjected to boundary tension, bending and domain pressure. The geometry of the shell is defined by the parameters $\mathbf{X} = [W_1, L_1, R_1, W_2, L_2, R_2, h, \kappa]$ and the design variables are $\mathbf{d} = [W_2, L_2, R_2, h, \kappa]$. In addition, the loading and material properties were treated as random variables, these were the bending moment $M$, tension $N$, domain pressure $P$ and yield strength $\sigma_Y$. The details of these variables are given in Table 8.

The BEM mesh of this structure is composed of 112 quadratic elements on the boundaries and 78 DRM points in the domain. The optimisation problem is defined such that the mass is to be minimised while a specific target reliability index $\beta_{target}$ is reached.

$$\begin{aligned} &\text{Minimise:} && Mass(\mathbf{d}) \\ &\text{Subject to:} && \mathbf{d}^L \le \mathbf{d} \le \mathbf{d}^U, \quad \mathbf{d} \in \mathbf{R}^5 \\ & && g(\mathbf{Z}) \le 0 \qquad (\|u\| = \beta_{target}) \end{aligned} \tag{49}$$

where the limit state function is defined as:

$$g(\mathbf{Z}) = \sigma_v^{max}(\mathbf{Q}) - \sigma_Y \tag{50}$$

where $\mathbf{Z} = [W_2, L_2, R_2, h, \kappa, M, N, P, \sigma_Y]$ and $\mathbf{Q} = [W_2, L_2, R_2, h, \kappa, M, N, P]$. The mass of the structure can be calculated using the parameters in $\mathbf{X}$ and density $\rho = 2700$ kgm$^{-3}$. The initial design is $\mathbf{d}_0 = [0.5, 0.25, 0.05, 0.05, 0.1]$ with the lower and upper bound $\mathbf{d}^L = 0.8\mathbf{d}_0$ and $\mathbf{d}^U = 1.2\mathbf{d}_0$, A wider range of the design variation was assigned for $R_2$ such that $\mathbf{d}^L_{R_2} = 0.03$ and $\mathbf{d}^U_{R_2} = 0.07$.

The optimisation of the shell structure was conducted with a range of reliability index targets $\beta_{target}$, whereby a higher $\beta_{target}$ indicates a lower probability of failure. The variation in the value of $\beta_{target}$ represents the safety requirements for a range of possible applications. It is expected that as the safety requirement increases, the mass of the optimised design will be larger.

The results of the optimisation for different target reliability indexes $\beta_{target}$ are given in the Table 9 and the iteration history of the optimisation is shown in Fig. 9. To verify that the optimal design is meeting the target reliability index, the true reliability index $\beta_{FORM}$ was evaluated using the FORM. It can be seen that the error between the $\beta_{target}$ and $\beta_{FORM}$ is less than 0.47%, meaning that $\beta_{target}$ and $\beta_{FORM}$ are in very good agreement. As the target reliability index increases, the optimal mass is higher which matches the expectation discussed earlier. The optimal geometry for $\beta_{target} = 2$ and $\beta_{target} = 6$ is shown in Fig. 10. As $\beta_{target}$ increases, optimal design becomes thicker and has higher curvature, the radius of the fillet is also larger and the 'window' section is smaller.

The maximum Von Mises stress occurs at the corner of the window. Therefore, the sensitivity of the maximum Von Mises stress to the size of the fillet $R_2$ is of particular interest. Sensitivity analysis can be performed at a specific reliability level (i.e. fixed $\beta_{target}$) to investigate the sensitivity of the maximum Von Mises stress with respect to the change in fillet radius. The derivatives of the maximum Von Mises stress with respect to the change in fillet radius using the optimal design parameters for $\beta_{target} = 4$ are shown in Fig. 11. The design variables are fixed at the optimal design results given in Table 9 while changing the value of $R_2$. The maximum Von Mises stress is less sensitive to the fillet radius when a larger $R_2$ was used in the design. The reliability index remains very close the target reliability index.

## 6. Conclusion

This paper presented a novel methodology for conducting reliability analyses using a newly developed Boundary Element Method-based Implicit Differentiation Method (BEM-IDM) for shallow shell structures. The BEM formulations for evaluating the response sensitivities with respect to changes in geometrical variables, curvature and thickness is proposed for the first time.

**Table 7**
Optimisation results from the IDM-based BEM with multiple Aluminium alloys.

| Material | $\sigma_Y$ [MPa] | Optimal volume [$m^3$] | Optimal mass [kg] | $r_2$ [m] | $\kappa$ [$m^{-1}$] | $h$ [m] |
|---|---|---|---|---|---|---|
| Aluminium 6061-T6 | 276 | 1.31 | 3536.3 | 4.621 | 0.00802 | 0.0197 |
| Aluminium 2024-T4 | 324 | 1.13 | 3133.6 | 4.500 | 0.00882 | 0.0179 |
| Aluminium 7050-T7 | 469 | 0.961 | 2719.8 | 4.501 | 0.00781 | 0.0153 |
| Aluminium 7075-T6 | 503 | 0.956 | 2687.7 | 4.539 | 0.00677 | 0.0150 |

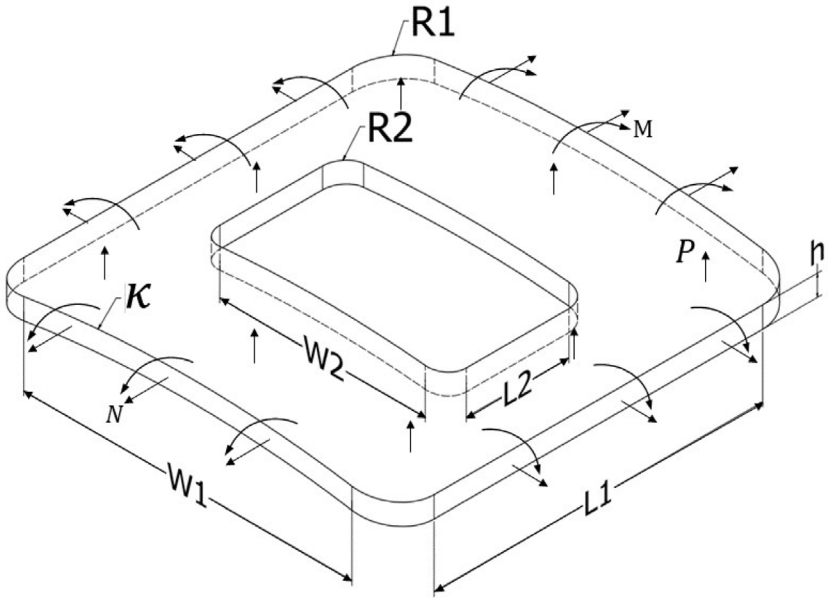


**Fig. 8.** Shell structure subjected at tension, bending and domain pressure loading.

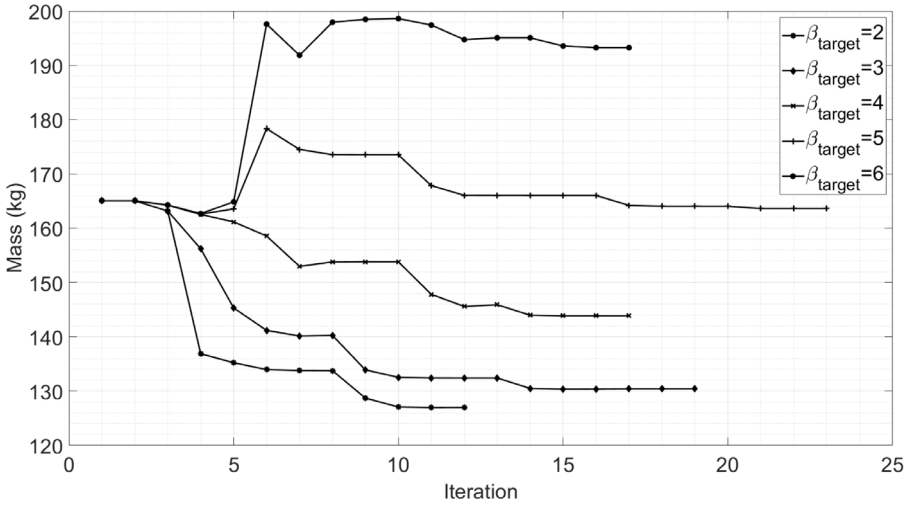


**Fig. 9.** Optimisation history from the IDM-based BEM with different target reliability $\beta_{target}$.

The exact derivatives of the BEM formulations were employed with the FORM for assessing the reliability of shell structures and the sensitivity of the failure criterion with respect to the changes in random variables. The IDM formulations were first validated using an analytical example featuring a hemispherical shell. The results show that the derivatives estimated from the BEM-IDM formulations compared very well with the analytical solution 2.61%. The IDM formulations were then used in the FORM for a structure featuring a circular shallow shell with an inner hole subjected to uniform pressure. The geometric variables, material properties, and applied pressure were treated as random variables. The influence of the changes in the curvature uncertainties on the structure reliability was investigated, and it was found that increasing the uncertainty in the curvature resulted in a higher probability of failure of the structure. The IDM results also shown good agreement with the results obtained from the FDM-FORM. The results from the IDM are very close to those obtained from the FDM with maximum difference of 0.11%. In order to investigate the impact of different variables on the reliability of the structure, a sensitivity analysis was conducted using the newly developed BEM-IDM. The results indicate that more effort should be devoted to controlling the uncertainties associated with geometrical variables as well as quantifying the uncertainties associated with pressure load.

To demonstrate how the BEM-IDM could be used in practice, it was employed as gradient-based optimisation procedure, which aimed to

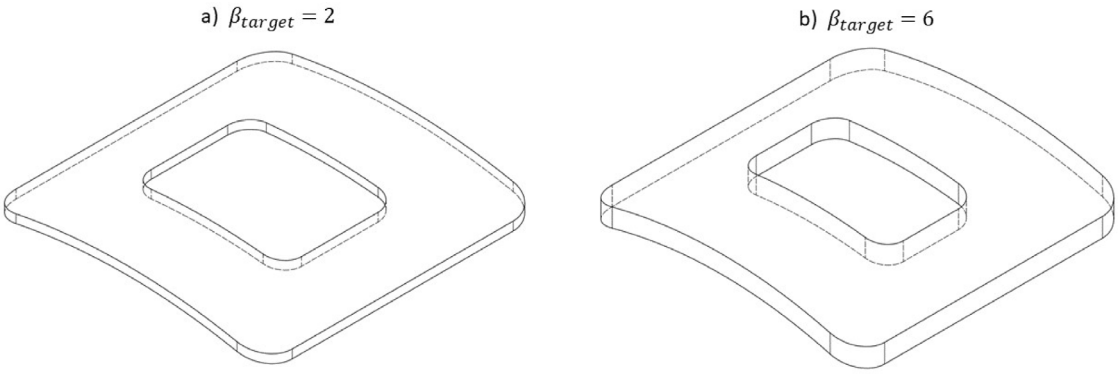


**Fig. 10.** Optimisation results for shell design with $\beta_{target} = 2$ and $\beta_{target} = 6$. (not to scale).

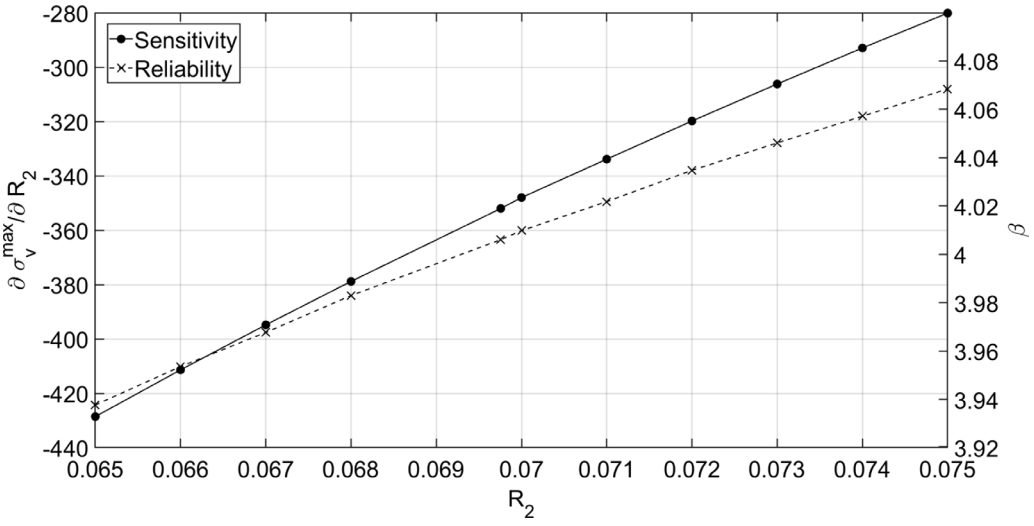


**Fig. 11.** Sensitivity of the maximum Von Mises stress to the change in fillet radius $R_2$ at the optimal design of $\beta_{target} = 4$.

**Table 8**
Details of the shell structure parameters and random variables used in the optimisation procedure.

| Variable | Description | Mean | CoV | Units |
|---|---|---|---|---|
| $W_1$ | Outer width | 1 | 0 | m |
| $L_1$ | Outer length | 1 | 0 | m |
| $R_1$ | Outer radius | 0.1 | 0 | m |
| $W_2$ | Inner width | 0.5 | 0.01 | m |
| $L_2$ | Inner length | 0.25 | 0.01 | m |
| $R_2$ | Inner radius | 0.05 | 0.01 | m |
| $h$ | Thickness | 0.05 | 0.01 | m |
| $\kappa$ | Curvature | 0.1 | 0.01 | $m^{-1}$ |
| $N$ | Boundary traction | 0.9 | 0.1 | MN $m^{-1}$ |
| $M$ | Boundary moment | 0.01 | 0.1 | MN |
| $P$ | Domain pressure | 0.056 | 0.1 | MPa |
| $\sigma_Y$ | Yield stress | 276 | 0.1 | MPa |

minimise mass, whilst maintaining a high-level of safety. A variety of materials with different yield strengths were used to investigate the effect of yield strength on the optimisation results. It is found that when stronger material were used, the optimal structure had lower mass. An optimisation example featuring Reliability-Based Design Optimisation (RBDO) was also investigated. It is found that when increasing the targeting reliability index, the mass of the structure increased to meet the stricter safety requirement. However, the method has inherent limitations in that the exactness of the probability of failure obtained from the FORM relies on the linearity or close-to-linearity of the limit state function in the variable space. To improve the accuracy of FORM results, methods such as the Second-Order Reliability Method (SORM) becomes favourable, as it approximates the limit state function through a second-order Taylor expansion. Nevertheless, employing SORM entails an increase in computational demand, as the computation of second-order derivatives of the BEM must be performed for each reliability analysis. In cases involving highly non-linear limit state functions, convergence issues have been observed in RBDO. However, the FORM has demonstrated sufficient accuracy for the majority of static structures.

Future work will focus on the application of IDM to the reliability analysis and optimisation of more complex structures, such as an aircraft fuselage. Fatigue crack growth and its impact on the reliability of shallow shell structures will also be investigated.

## Declaration of competing interest

The authors declare that they have no known competing financial interests or personal relationships that could have appeared to influence the work reported in this paper.

## Data availability

Data will be made available on request

## Acknowledgements

This research did not receive any specific grant from funding agencies in the public, commercial, or not-for-profit sectors.

**Table 9**
Optimisation results for different target reliability indexes $\beta_{target}$.

| $\beta_{target}$ | $W_2$ | $L_2$ | $R_2$ | $h$ | $\kappa$ | Mass [kg] | $\beta_{FORM}$ | $P_f$ (%) |
|---|---|---|---|---|---|---|---|---|
| Initial design | 0.5 | 0.25 | 0.05 | 0.05 | 0.1 | 165.1 | 3.651 | 0.01311 |
| 2 | 0.4970 | 0.2892 | 0.06956 | 0.04006 | 0.1179 | 125.4 | 2.008 | 2.232 |
| 3 | 0.4050 | 0.2771 | 0.06967 | 0.04008 | 0.1192 | 130.4 | 3.014 | 0.1289 |
| 4 | 0.4012 | 0.2064 | 0.06976 | 0.04279 | 0.1196 | 143.9 | 4.006 | 0.003088 |
| 5 | 0.4002 | 0.2009 | 0.06996 | 0.04856 | 0.1199 | 163.6 | 5.001 | 2.852e−05 |
| 6 | 0.4007 | 0.2027 | 0.06983 | 0.05739 | 0.1196 | 193.3 | 6.003 | 9.805e−08 |

## Appendix A

The derivation and detailed expressions for the particular solutions used in the DRM method can be found in [33] for the transformation of the domain integral to the boundary integral. The derivatives of the particular solutions with respect to some geometry variables $Z_g$ are derived for the first time in this work and are shown below.

The distance between the field point and collocation point can be found by:

$$r = \sqrt{(x_1 - x_1')^2 + (x_2 - x_2')^2} \tag{51}$$

where $x_1$ and $x_2$ represent the x and y coordinates of the nodal points respectively. Therefore, the derivatives of $r$ can be found by:

$$r_{,g} = \left((x_1 - x_1')(x_{1,g} - x_{1,g}') + (x_2 - x_2')(x_{2,g} - x_{2,g}')\right)/r \tag{52}$$

### *A.1. Derivatives of the particular solutions for 2D plane stress with respect to a geometrical variable*

The derivatives of the particular solution for displacement are:

$$\begin{aligned}
\hat{u}^1_{m1,g} &= -\frac{2}{(1-\nu)B}\left[\frac{1}{3}\left(r_{,g}x_1 + r x_{1,g}\right) - \frac{1+\nu}{30}\left(\frac{1}{r^2}\left(3x_1x_{1,g}r - x_1^3 r_{,g}\right)\right.\right.\\
&\left.\left. +3x_{1,g}r + 3x_1 r_{,g}\right)\right]\\
\hat{u}^1_{m2,g} &= \frac{(1+\upsilon)}{15(1-\upsilon)B}\left[\frac{1}{r^2}\left(2x_1x_{1,g}x_2 r + x_1^2 x_{2,g}r - r_{,g}x_1^2x_2\right) + x_{2,g}r + x r_{,g}\right]\\
\hat{u}^2_{m1,g} &= \frac{1+\nu}{15(1-\nu)B}\left[\frac{1}{r^2}\left(2x_2x_{2,g}x_1 r + x_2^2 x_{1,g}r - r_{,g}x_2^2x_1\right) + x_{1,g}r + x r_{,g}\right]\\
\hat{u}^2_{m2,g} &= -\frac{2}{(1-\nu)B}\left[\frac{1}{3}\left(r_{,g}x_2 + r x_{2,g}\right) - \frac{1+\nu}{30}\left(\frac{1}{r^2}\left(3x_2^2x_{2,g}r\right.\right.\right.\\
&\left.\left.\left. -x_2{}^3 r_{,g}\right) + 3x_{2,g}r + 3x r_{,g}\right)\right]
\end{aligned} \tag{53}$$

The derivatives of the particular solutions for the strains are:

$$\begin{aligned}
\hat{\varepsilon}^1_{m11,g} &= -\frac{2}{(1-\nu)}\left[\frac{1}{r^2}\left(2x_1x_{1,g}r - r_{,g}x_1^2\right) + \frac{1}{3}r_{,g} - \frac{1+\nu}{30}\left(-\frac{1}{r^6}\left(4x_1^3x_{1,g}r^3\right.\right.\right.\\
&\left.\left.\left. -3r^2r_{,g}x_1^4\right) + \frac{1}{r^2}\left(12x_1x_{1,g}r - 6x_1^2r_{,g}\right) + 3r_{,g}\right)\right]\\
\hat{\varepsilon}^1_{m12,g} &= -\frac{2}{(1-\nu)}\left[\frac{1}{6r^2}\left(x_{1,g}x_2r + x_1x_{2,g}r - r_{,g}x_1x_2\right) - \frac{(1+\nu)}{30}\left(-\frac{1}{r^6}\left(3x_1^2x_{1,g}x_2r^3\right.\right.\right.\\
&\left.\left.\left. +x_1^3x_{2,g}r^3\right) + \frac{3}{r^6}x_1^3x_2r^2r_{,g} + \frac{1}{r^2}\left(3x_{1,g}x_2r + 3x_1x_{2,g}r - 3x_1x_2r_{,g}\right)\right)\right]\\
\hat{\varepsilon}^1_{m22,g} &= \frac{(1+\nu)}{15(1-\nu)}\left[-\frac{1}{r^6}\left(2x_1x_{1,g}x_2^2r^3 + 2x_1^2x_2x_{2,g}r^3 - 3x_1^2x_2^2r^2r_{,g}\right) + 2r_{,g}\right]\\
\hat{\varepsilon}^2_{m11,g} &= \frac{(1+\nu)}{15(1-\nu)}\left[-\frac{1}{r^6}\left(2x_1x_{1,g}x_2^2r^3 + 2x_1^2x_2x_{2,g}r^3\right.\right.\\
&\left.\left. -3r^2r_{,g}x_1{}^2x_2{}^2\right) + 2r_{,g}\right]\\
\hat{\varepsilon}^2_{m12,g} &= -\frac{2}{(1-\nu)}\left[\frac{1}{6r^2}\left(x_{1,g}x_2r + x_1x_{2,g}r - r_{,g}x_1x_2\right) - \frac{1+\nu}{30}\left(-\frac{1}{r^6}\left(3x_2^2x_{2,g}x_1r^3\right.\right.\right.\\
&\left.\left.\left. +x_2{}^3x_{1,g}r^3 - 3x_2^3x_1r^2r_{,g}\right) + \frac{1}{r^2}\left(3x_{1,g}x_2r + 3x_1x_{2,g}r - 3x_1x_2r_{,g}\right)\right)\right]\\
\hat{\varepsilon}^2_{m22,g} &= -\frac{2}{1-\nu}\left[\frac{1}{r^2}\left(2x_2x_{2,g}r - r_{,g}x_2^2\right) + \frac{1}{3}r_{,g} - \frac{1-\nu}{30}\left(-\frac{1}{r^6}\left(4x_2^3x_{2,g}r^3\right.\right.\right.\\
&\left.\left.\left. +3x_2^4r^2r_{,g}\right) + \frac{1}{r^2}\left(12x_2x_{2,g}r - 6x_2^2r_{,g}\right) + 3r_{,g}\right)\right]
\end{aligned} \tag{54}$$

The derivatives of the particular solution for the membrane stress are: resultant $\hat{N}_{m\alpha\beta}$

$$\begin{aligned}
\hat{N}^{ii}_{m11,g} &= B\left[(1-\upsilon)\hat{\varepsilon}^{ii}_{m11,g} + \upsilon\hat{\varepsilon}^{ii}_{m11,g} + \upsilon\hat{\varepsilon}^{ii}_{m22,g}\right]\\
\hat{N}^{ii}_{m12,g} &- B(1-\nu)\hat{\varepsilon}^{ii}_{m12,g}\\
\hat{N}^{ii}_{m22,g} &= B\left[(1-\nu)\hat{\varepsilon}^{ii}_{m22,g} + \nu\hat{\varepsilon}^{ii}_{m11,g} + \nu\hat{\varepsilon}^{ii}_{m22,g}\right]
\end{aligned} \tag{55}$$

The particular solutions for traction can be found by multiplying the membrane stress resultant with the unit outward normal such that $\hat{t}_{m\alpha} = \hat{N}_{m\alpha\beta}n_\beta$. The derivatives of the traction can be found by:

$$\hat{t}^{ii}_{m\alpha,g} = \hat{N}^{ii}_{m\alpha\beta,g}n_\beta + \hat{N}^{ii}_{m\alpha\beta}n_{\beta,g} \tag{56}$$

In the above equation, superscript $ii$ can take values of 1 or 2.

### *A.2. Derivatives of the particular solutions for plate bending with respect to a geometrical variable*

From the bending stress resultant-displacement relationship, the tractions on the boundary can be found by the bending moment stress resultants $\hat{M}_{m\alpha\beta}$ and shear force stress resultants $\hat{Q}_{m\alpha}$ such that:

$$\hat{p}_{m\alpha} = \hat{M}_{m\alpha\beta}n_\beta, \qquad \hat{p}_{m3} = \hat{Q}_{m\alpha}n_\alpha \tag{57}$$

The derivatives of the tractions can be found by:

$$\hat{p}_{m\alpha,g} = \hat{M}_{m\alpha\beta,g}n_\beta + \hat{M}_{m\alpha\beta}n_{\beta,g}, \qquad \hat{p}_{m3,g} = \hat{Q}_{m\alpha,g}n_\alpha + \hat{Q}_{m\alpha}n_{\alpha,g} \tag{58}$$

For the function $F_{,\alpha} = x_\alpha/r$, the derivatives of the particular solution when $\alpha = 1$ can be calculated as:

$$\begin{aligned}
\iota\hat{w}^1_{m1,g} &= -\left(r_{,g}\left(3x_1^2 + r^2\right) + r\left(6x_1x_{1,g} + 2rr_{,g}\right)\right)\frac{1}{45D}\\
\iota\hat{w}^1_{m2,g} &= -\left(x_1x_2r_{,g} + x_1x_{2,g}r + x_{1,g}x_2r\right)\frac{1}{15D}\\
\iota\hat{w}^1_{m3,g} &= -\left[30 - (1-\nu)\lambda^2\right]\frac{r_{,g}x_1 + rx_{1,g}}{45(1-\nu)\lambda^2 D} + \left[(1-\nu)\lambda^2 2rr_{,g}\right]\frac{rx_1}{45(1-\nu)\lambda^2 D}
\end{aligned} \tag{59}$$

where bending stiffness $D = Eh^3/[12(1-\nu^2)]$ and $\lambda = \sqrt{10}/h$. the derivatives for the particular solutions of moments $\hat{M}_{\alpha\beta}$ and shear forces $\hat{Q}_\beta$ are:

$$\begin{aligned}
\hat{M}^1_{m11,g} &= S^1_{11}g + \nu S^1_{22,g}\\
\hat{M}^1_{m12,g} &= (1-\nu)S^1_{12,g}\\
\hat{M}^1_{m22,g} &= \nu S^1_{11,g} + S^1_{22,g}
\end{aligned} \tag{60}$$

where:

$$\begin{aligned}
S^1_{11,g} &= -\frac{1}{15}\left[\frac{1}{r^2}\left(3x_1^2x_{1,g}r - x_1^3r_{,g}\right) + 3r_{,g}x_1 + 3rx_{1,g}\right]\\
S^1_{12,g} &= -\frac{1}{15}\left[\frac{1}{r^2}\left(2x_1x_{1,g}x_2r + x_1^2x_{2,g}r - x_1^2x_2r_{,g}\right) + r_{,g}x_2 + rx_{2,g}\right]\\
S^1_{22,g} &= -\frac{1}{15}\left[\frac{1}{r^2}\left(2rx_2x_{2,g}x_1 + rx_2{}^2x_{1,g} - x_2^2x_1r_{,g}\right) + r_{,g}x_1 + rx_{1,g}\right]
\end{aligned} \tag{61}$$

$$\begin{aligned}
\hat{Q}^1_{m1,g} &= -\frac{1}{3}\left(r_{,g} + 2x_1x_{1,g}\frac{1}{r} - x_1^2r_{,g}\frac{1}{r^2}\right)\\
\hat{Q}^1_{m2,g} &= -\frac{1}{3}\left(\frac{1}{r}x_1x_{2,g} + \frac{1}{r}x_2x_{1,g} - \frac{1}{r^2}x_1x_2r_{,g}\right).
\end{aligned} \tag{62}$$

For $\alpha = 2$, the derivatives of the particular solutions are:

$$\begin{aligned}
\hat{w}^2_{m_1,g} &= -\frac{1}{15D}\left(x_{1,g}x_2 r + x_1 x_{2,g} r + x_1 x_2 r_{1,g}\right)\\
\hat{w}^2_{m2,g} &= -\frac{1}{45D}\left[\left(6x_2 x_{2,g} + 2rr_{,g}\right)r - \left(3x_2^2 + r^2\right)r_{,g}\right]\\
\hat{w}^2_{m3,g} &= -\left[30 - (1-\nu)\lambda^2 r^2\right]\frac{r_g x_2 + r x_{2,g}}{45(1-\nu)\lambda^2 D} + (1-\nu)\lambda^2 2rr_{,g}\frac{r x_2}{45(1-\nu)\lambda^2 D}
\end{aligned} \tag{63}$$

The derivatives for the particular solutions of moments $\hat{M}_{\alpha\beta}$ and shear forces $\hat{Q}_{beta}$ are:

$$\begin{aligned}
\hat{M}^2_{m11,g} &= S^2_{11,g} + \nu S^2_{22,g}\\
\hat{M}^2_{m12,g} &= (1-\nu)S^2_{12,g}\\
\hat{M}^2_{m22,g} &= \nu S^2_{11,g} + S^2_{22,g}
\end{aligned} \tag{64}$$

where:

$$\begin{aligned}
S^2_{11,g} &= -\frac{1}{15D}\left[\frac{1}{r^2}\left(2x_1 x_{1,g} x_2 r + x_1^2 x_{2,g} r - x_1^2 x_2 r_{,g}\right) + r_{,g}x_2 + r x_{2,g}\right]\\
S^2_{12,g} &= -\frac{1}{15D}\left[\frac{1}{r^2}\left(x_{1,g}x_2^2 r + 2x_1 x_2 x_{2,g} r - x_1 x_2^2 r_{,g}\right) + r_{,g}x_1 + r x_{1,g}\right]\\
S^2_{22,g} &= -\frac{1}{15D}\left[\frac{1}{r^2}\left(3x_2^2 x_{2,g} r - x_2^3 r_{,g}\right) + 3r x_{2,g} + 3r_{,g}x_2\right]
\end{aligned} \tag{65}$$

$$\begin{aligned}
\hat{Q}^2_{m1,g} &= -\frac{1}{3}\left[\frac{1}{r}\left(x_1 x_{2,g}\right) + \frac{1}{r}x_2 x_{1,g} - \frac{1}{r^2}x_1 x_2 r_{,g}\right]\\
\hat{Q}^2_{m2,g} &= -\frac{1}{3}\left(r_{,g} + 2x_2 x_{2,g}\frac{1}{r} - x_2^2 r_{,g}\frac{1}{r^2}\right).
\end{aligned} \tag{66}$$

For the radial basis function $F(r) = 1+r$, the derivatives of the rotations and deflection can be calculated by:

$$\begin{aligned}
\hat{w}^3_{m1,g} &= -\frac{1}{D}\left(\frac{1}{16} + \frac{r}{45}\right)\left(x_{1,g}r^2 + 2rr_{,g}x_1\right) - \frac{1}{45D}\left(r_{,g}x_1 r^2\right)\\
\hat{w}^3_{m2,g} &= -\frac{1}{D}\left(\frac{1}{16} + \frac{r}{45}\right)\left(x_{2,g}r^2 + 2rr_{,g}x_2\right) - \frac{1}{45D}x_2 r^2 r_{,g}\\
\hat{w}^3_{m3,g} &= -\left(\frac{1}{2} + \frac{2r}{9}\right)\frac{2rr_{,g}}{(1-\nu)\lambda^2 D} - \frac{2r_{,g}}{9}\frac{r^2}{(1-\nu)\lambda^2 D} + \frac{r_{,g}}{225D}
\end{aligned} \tag{67}$$

The derivatives of the particular solutions of moment $\hat{M}_{m\alpha\beta}$ can be derived:

$$\begin{aligned}
\hat{M}^3_{m11,g} &= -\left[\frac{r_{,g}}{15}\left(x_1^2 + \nu x_2^2\right) + \left(\frac{1}{8} + \frac{r}{15}\right)\left(2x_1 x_{1,g} + 2\nu x_2 x_{2,g}\right)\right.\\
&\quad \left.+(1+\nu)\left(\frac{1}{8}rr_{,g} + \frac{1}{15}r^2 r_{,g}\right)\right]\\
\hat{M}^3_{m12,g} &= -(1+\nu)\frac{1}{15}r_{,g}x_1 x_2 - (1+\nu)\left(\frac{1}{8} + \frac{r}{15}\right)\left(x_{1,g}x_2 + x_1 x_{2,g}\right)\\
\hat{M}^3_{m22,g} &= -\left[\frac{1}{15}r_{,g}\left(\nu x_1^2 + x_2^2\right) + \left(\frac{1}{8} + \frac{r}{15}\right)\left(20\nu x_1 x_{1,g} + 2x_2 x_{2,g}\right)\right.\\
&\quad \left.+(1+\nu)\left(\frac{1}{8}rr_{,g} + \frac{1}{15}r^2 r_{,g}\right)\right]
\end{aligned} \tag{68}$$

The derivatives of the shear forces $\hat{Q}_{m\beta}$ are:

$$\begin{aligned}
\hat{Q}^3_{m1,g} &= -\frac{x_{1,g}}{2}\left(1 + \frac{2r}{3}\right) - \frac{1}{3}x_1 r_{,g}\\
\hat{Q}^3_{m2,g} &= -\frac{x_{2,g}}{2}\left(1 + \frac{2r}{3}\right) - \frac{1}{3}x_2 r_{,g}
\end{aligned} \tag{69}$$

## Appendix B

The derivatives of the particular solutions with respect to the thickness are needed in the DRM for transforming the domain integral into boundary integral. The derivatives of the BEM membrane and bending fundamental solutions with respect to the thickness were proposed in the previous literature [21]. Here, only the derivatives of the particular solutions for shell BEM is presented.

The coefficient related to the BEM integrals are defined as:

$$\begin{aligned}
B &= Eh/(1-\nu^2)\\
D &= Eh^3/12(1-\nu^2)\\
CW &= 45(1-\nu)\lambda^2 D\\
\lambda &= \sqrt{(10)}/h
\end{aligned} \tag{70}$$

The derivatives with respect to the thickness are:

$$\begin{aligned}
B_{,h} &= B/h\\
D_{,h} &= 3D/h\\
CW_{,h} &= 45(1-\nu)(D_{,h}\lambda^2 + 2D\lambda\lambda_{,h})\\
\lambda_{,h} &= -\lambda/h
\end{aligned} \tag{71}$$

### *B.1. Derivatives of the particular solutions for 2D plane stress with respect to thickness*

The derivatives of the particular solution for displacement:

$$\begin{aligned}
\hat{u}^1_{m1,h} &= \frac{2B_{,h}}{(1-\nu)B^2}\left[\frac{r x_1}{3} - \frac{1+\nu}{30}\left(\frac{x_1^3}{r} + 3x_1 r\right)\right]\\
\hat{u}^1_{m2,h} &= -\frac{(1+\nu)B_{,h}}{15(1-\nu)B^2}\left(\frac{x_1^2 x_2}{r} + x_2 r\right)\\
\hat{u}^2_{m1,h} &= -\frac{(1+\nu)B_{,h}}{15(1-\nu)B^2}\left(\frac{x_2^2 x_1}{r} + x_1 r\right)\\
\hat{u}^2_{m2,h} &= \frac{2B_{,h}}{(1-\nu)B^2}\left[\frac{r x_2}{3} - \frac{1+\nu}{30}\left(\frac{x_2^3}{r} + 3x_2 r\right)\right]
\end{aligned} \tag{72}$$

The derivatives of the particular solution for the membrane stress resultant

$$\begin{aligned}
\hat{N}^{ii}_{m11,g} &= B_{,h}\left[(1-\nu)\hat{\varepsilon}^{ii}_{m11} + \nu\hat{\varepsilon}^{ii}_{m11} + \nu\hat{\varepsilon}^{ii}_{m22}\right]\\
\hat{N}^{ii}_{m12,g} &= B_{,h}(1-\nu)\hat{\varepsilon}^{ii}_{m12}\\
\hat{N}^{ii}_{m22,g} &= B_{,h}\left[(1-\nu)\hat{\varepsilon}^{ii}_{m22} + \nu\hat{\varepsilon}^{ii}_{m11} + \nu\hat{\varepsilon}^{ii}_{m22}\right]
\end{aligned} \tag{73}$$

where the superscript $ii$ can take a value of 1 or 2.

### *B.2. Derivatives of the particular solution for plate bending with respect to thickness*

The derivatives of the particular solution when $\alpha = 1$ are:

$$\begin{aligned}
\hat{w}^1_{m1,h} &= \left(3x_1^2 + r^2\right)\frac{r D_{,h}}{45D^2}\\
\hat{w}^1_{m2,h} &= \frac{x_1 x_2 r D_{,h}}{15D^2}\\
\hat{w}^1_{m3,h} &= \left[30 - (1-\nu)\lambda^2 r^2\right]\frac{r x_1 \cdot CW_{,h}}{CW^2} + (2x_1 r^3\lambda\lambda_{,h}(1-\nu))\frac{1}{CW}
\end{aligned} \tag{74}$$

For $\alpha = 2$:

$$\begin{aligned}
\hat{w}^2_{m1,h} &= \frac{x_1 x_2 r D_{,h}}{15D^2}\\
\hat{w}^2_{m2,h} &= \left(3x_2^2 + r^2\right)\frac{r D_{,h}}{45D^2}\\
\hat{w}^2_{m3,h} &= \left[30 - (1-\nu)\lambda^2 r^2\right]\frac{x_2 r CW_{,h}}{CW^2} + (2x_2 r^3\lambda\lambda_{,h}(1-\nu))\frac{1}{CW}
\end{aligned} \tag{75}$$

For $\alpha = 3$:

$$\begin{aligned}
\hat{w}^3_{m1,h} &= \left(\frac{1}{16} + \frac{r}{45}\right)\frac{x_1 r^2 D_{,h}}{D^2}\\
\hat{w}^3_{m2,h} &= \left(\frac{1}{16} + \frac{r}{45}\right)\frac{x_2 r^2 D_{,h}}{D^2}\\
\hat{w}^3_{m3,h} &= -\left(\frac{1}{64} + \frac{r}{225}\right)\frac{D_{,h}}{D^2} + \left(\frac{1}{2} + \frac{2r}{9}\right)\frac{r^2 D_{,h}}{(1-\nu)\lambda^2 D^2}\\
&\quad + \left(\frac{1}{2} + \frac{2r}{9}\right)\frac{2r^2\lambda_{,h}}{(1-\nu)\lambda^3 D}
\end{aligned} \tag{76}$$

## Appendix C

The detailed formulations for the derivatives of the boundary stress resultants are given in this section with respect to geometrical parameters, curvature and thickness, respectively.

### C.1. Bending stress resultant derivatives

(1) With respect to $g$:

$$\begin{aligned}
&\hat{M}_{11,g} = \hat{p}_{1,g}, \qquad \hat{M}_{12,g} = \hat{p}_{2,g} \\
&\hat{M}_{22,g} = \nu\hat{M}_{11,g} + D\left(1-\nu^2\right)\hat{\chi}_{22,g} \\
&\hat{\chi}_{22,g} = \frac{1}{J(\zeta)}\left[e_{2\alpha,g}\sum\left(\hat{w}_\alpha\left(\frac{dN(\zeta)}{d\zeta}\right)\right) - J_{,g}(\zeta)\hat{\chi}_{22}\right. \\
&\quad \left. + e_{2\alpha}\sum\left(\hat{w}_{\alpha,g}\left(\frac{dN(\zeta)}{d\zeta}\right)\right)\right]
\end{aligned} \tag{77}$$

(2) With respect to $K$:

$$\begin{aligned}
&\hat{M}_{11,\rho} = \hat{p}_{1,\rho} \quad \hat{M}_{12,\rho}\rho = \hat{p}_{2,\rho} \\
&\hat{M}_{22,\rho} = \nu\hat{M}_{11,\rho} + D\left(1-\nu^2\right)\hat{\chi}_{22,\rho} \\
&\hat{\chi}_{22,\rho} = \frac{e_{2\alpha}}{J(\zeta)}\sum\left(\hat{w}_{\alpha,\rho}\left(\frac{dN(\zeta)}{d\zeta}\right)\right)
\end{aligned} \tag{78}$$

(3) With respect to $h$:

$$\begin{aligned}
&\hat{M_{11,h}} = \hat{p}_{1,h} \quad \hat{M}_{12,h} = \hat{p}_{2,h} \\
&\hat{M_{22,h}} = \nu\hat{M_{11,h}} + D_{,h}\left(1-\nu^2\right)\hat{\chi}_{22} + D\left(1-\nu^2\right)\hat{\chi}_{22,h} - \frac{2\lambda_{,h}q_3 v}{\lambda^3}
\end{aligned} \tag{79}$$

### C.2. Shear stress resultant derivatives

(1) With respect to $g$:

$$\begin{aligned}
&\hat{Q}_{1,g} = \hat{p}_{3,g} \\
&\hat{Q}_{2,g} = \frac{D(1-\nu)\lambda^2}{2}\left[w_{2,g} + \frac{1}{J(\zeta)}\sum\left(w_{3,g}\left(\frac{dN(\zeta)}{d\zeta}\right)\right)\right. \\
&\quad \left. - \frac{J_{,g}(\zeta)}{J^2(\zeta)}\sum\left(w_3\left(\frac{dN(\zeta)}{d\zeta}\right)\right)\right]
\end{aligned} \tag{80}$$

(2) With respect to $k$:

$$\begin{aligned}
&\hat{Q}_{1,\rho} = \hat{p}_{3,\rho} \\
&\hat{Q}_{2,\rho} = \frac{D(1-\nu)\lambda^2}{2}\left[w_{2,\rho} + \frac{1}{J(\zeta)}\sum\left(w_{3,\rho}\left(\frac{dN(\zeta)}{d\zeta}\right)\right)\right]
\end{aligned} \tag{81}$$

(3) With respect to h:

$$\begin{aligned}
&\hat{Q_{1,h}} = \hat{p_{3,h}} \\
&\hat{Q}_{2,h} = \frac{D_{,h}(1-\nu)\lambda^2}{2}\left[w_2 + \frac{1}{J(\zeta)}\sum\left(w_3\left(\frac{dN(\zeta)}{d\zeta}\right)\right)\right] \\
&+ \frac{2D(1-\nu)\lambda\lambda_{,h}}{2}\left[w_2 + \frac{1}{J(\zeta)}\sum\left(w_3\left(\frac{dN(\zeta)}{d\zeta}\right)\right)\right] \\
&+ \frac{D(1-\nu)^2}{2}\left[w_{2,h} + \frac{1}{J(\zeta)}\sum\left(w_{3,h}\left(\frac{dN(\zeta)}{d\zeta}\right)\right)\right]
\end{aligned} \tag{82}$$

## References


[1] Wang X, Shi Q, Fan W, Wang R, Wang L. Comparison of the reliability-based and safety factor methods for structural design. Appl Math Model 2019;72:68–84. http://dx.doi.org/10.1016/j.apm.2019.03.018.

[2] Aliabadi MH. The boundary element method: applications in solids and structures, Vol. 2. John Wiley and Sons; 2002.

[3] Besterfield GH, Liu WK, Lawrence MA, Belytschko TB. Brittle fracture reliability by probabilistic finite elements. J Eng Mech 1990;116(3):642–59. http://dx.doi.org/10.1061/(ASCE)0733-9399(1990)116:3(642).

[4] Yoo K, Bacarreza O, Aliabadi MH. A novel multi-fidelity modelling-based framework for reliability-based design optimisation of composite structures. Eng Comput 2022;38:595–608. http://dx.doi.org/10.1007/s00366-020-01084-x.

[5] Zheng C, Zhao W, Gao H, Du L, Zhang Y, Bi C. Sensitivity analysis of acoustic eigenfrequencies by using a boundary element method. J Acoust Soc Am 2021;149(3):2027–39. http://dx.doi.org/10.1121/10.0003622.

[6] Fahmy MA, Alsulami MO. Boundary element and sensitivity analysis of anisotropic thermoelastic metal and alloy discs with holes. Materials (Basel, Switzerland) 2022;15(5):1828. http://dx.doi.org/10.3390/ma15051828.

[7] Tafreshi A. Shape sensitivity analysis of composites in contact using the boundary element method. Eng Anal Bound Elem 2009;33(2):215–24. http://dx.doi.org/10.1016/j.enganabound.2008.04.008.

[8] Sfantos GK, Aliabadi MH. A boundary element sensitivity formulation for contact problems using the implicit differentiation method. Eng Anal Bound Elem 2006;30(1):22–30. http://dx.doi.org/10.1016/j.enganabound.2005.08.004.

[9] Su C, Xu J. Reliability analysis of Reissner plate bending problems by stochastic spline fictitious boundary element method. Eng Anal Bound Elem 2015;51:37–43. http://dx.doi.org/10.1016/j.enganabound.2014.10.006.

[10] Kim D, Kwak B. Reliability-based shape optimization of two-dimensional elastic problems using BEM. Comput Struct 1996;60(5):743–50. http://dx.doi.org/10.1016/0045-7949(95)00433-5.

[11] Canelas A, Herskovits J, Telles JCF. Shape optimization using the boundary element method and a SAND interior point algorithm for constrained optimization. Comput Struct 2008;86(13):1517–26. http://dx.doi.org/10.1016/j.compstruc.2007.05.008, Structural Optimization.

[12] Tafresh A. Shape optimization of two-dimensional anisotropic structures using the boundary element method. J Strain Anal Eng Des 2003;38(3):219–32. http://dx.doi.org/10.1243/030932403765310554.

[13] Kala Z. Probability based global sensitivity analysis of fatigue reliability of steel structures. IOP Conf Ser: Mater Sci Eng 2019;668(1):012015. http://dx.doi.org/10.1088/1757-899X/668/1/012015.

[14] Lee O, Kim DH. Reliability of fatigue damaged structure using FORM, SORM and fatigue model. In: World congress on engineering. 2007.

[15] Melchers RE, Ahammed M. A fast approximate method for parameter sensitivity estimation in Monte Carlo structural reliability. Comput Struct 2004;82:55–61.

[16] Besterfield GH, Liu W, Lawrence MA, Belytschko T. Fatigue crack growth reliability by probabilistic finite elements. Comput Methods Appl Mech Engrg 1991;86(3):297–320. http://dx.doi.org/10.1016/0045-7825(91)90225-U.

[17] Kim Dong Won, Kwak Byung Man. Reliability-based shape optimization of two-dimensional elastic problems using BEM. Comput Struct 1996;60(5):743–50. http://dx.doi.org/10.1016/0045-7949(95)00433-5.

[18] Huang X, Aliabadi MH. A boundary element method for structural reliability. Key Eng Mater 2015;627:453–6. http://dx.doi.org/10.4028/www.scientific.net/KEM.627.453.

[19] Huang X, Aliabadi MH, Sharif Khodaei Z. Fatigue crack growth reliability analysis by stochastic boundary element method. CMES Comput Model Eng Sci 2014;102(4):291–330. http://dx.doi.org/10.3970/cmes.2014.102.291.

[20] Morse L, Sharif Khodaei Z, Aliabadi MH. Multi-fidelity modeling-based structural reliability analysis with the boundary element method. J Multiscale Model 2017;08:1740001. http://dx.doi.org/10.1142/S1756973717400017.

[21] Morse L, Mallardo V, Aliabadi MH. Manufacturing cost and reliability-based shape optimization of plate structures. Internat J Numer Methods Engrg 2022;123(10):2189–213. http://dx.doi.org/10.1002/nme.6931.

[22] Potrzeszcz-Sut B. Reliability analysis of shell truss structure by hybrid Monte Carlo method. J Theoret Appl Mech 2020;58(2):469–82. http://dx.doi.org/10.15632/jtam-pl/118886.

[23] Liu H, Li N. Reliability analysis of autonomous underwater vehicle aft pressure shell for optimal design and strength. Ocean Eng 2022;249:110906. http://dx.doi.org/10.1016/j.oceaneng.2022.110906.

[24] N. Sandipan, Chakraborty S, Ray C. Reliability analysis of laminated composite shells by response surface method based on HSD. Struct Eng Mech 2019;72(2):203–16. http://dx.doi.org/10.12989/sem.2019.72.2.203.

[25] Morse L, Sharif Khodaei Z, Aliabadi MH. A dual boundary element based implicit differentiation method for determining stress intensity factor sensitivities for plate bending problems. Eng Anal Bound Elem 2019;106:412–26. http://dx.doi.org/10.1016/j.enganabound.2019.05.021.

[26] Morse L, Mallardo V, Sharif-Khodaei Z, Aliabadi FMH. Shape optimisation of assembled plate structures with the boundary element method. Aerospace 2022;9:381. http://dx.doi.org/10.3390/aerospace9070381.

[27] Novozhilov VV. The theory of thin elastic shells. Groningen: P. Noordhoff Ltd; 1964.

[28] Naghdi PM. Note on the equations of shallow elastic shells. Quart Appl Math 1956;14:331–3.

[29] Reissner E. Stress strain relations in the theory of thin elastic shells. J Math Phys 1952;31:109–19. http://dx.doi.org/10.1002/sapm1952311109.

[30] Lu Pin P, Huang M. Boundary element analysis of shallow shells involving shear deformation. Int J Solids Struct 1992;29(10):1273–82. http://dx.doi.org/10.1016/0020-7683(92)90237-N.

[31] Wen P, Aliabadi MH, Young A. Transformation of domain integrals to boundary integrals in BEM analysis of shear deformable plate bending problems. Comput Mech 1999;24:304–9. http://dx.doi.org/10.1007/s004660050519.

[32] Dirgantara T, Aliabadi MH. A new boundary element formulation for shear deformable shells analysis. Internat J Numer Methods Engrg 1999;45(9):1257–75. http://dx.doi.org/10.1002/(SICI)1097-0207(19990730)45:9<1257::AID-NME629>3.0.CO;2-N.

[33] Dirgantara T, Aliabadi MH. Dual boundary element formulation for fracture mechanics analysis of shear deformable shells. Int J Solids Struct 2001;38(44):7769–800. http://dx.doi.org/10.1016/S0020-7683(01)00097-X.

[34] Mellings SC, Aliabadi MH. Three-dimensional flaw identification using inverse analysis. 34, (4):1996, p. 453–69. http://dx.doi.org/10.1016/0020-7225(95)00125-5,

[35] Mellings SC, Aliabadi MH. Flaw identification using the boundary element method. Internat J Numer Methods Engrg 1995;38(3):399–419. http://dx.doi.org/10.1002/nme.1620380304.
[36] G. Jia, Du X. Reliability sensitivity analysis with random and interval variables. Internat J Numer Methods Engrg 2009;78(13):1585–617. http://dx.doi.org/10.1002/nme.2543.
[37] Zhang Y, Der Kiureghian A. Two improved algorithms for reliability analysis. In: Rackwitz Rüdiger, Augusti Guiliano, Borri Antonio, editors. Reliability and optimization of structural systems: proceedings of the sixth IFIP WG7.5 working conference on reliability and optimization of structural systems 1994. Springer US; 1995, p. 297–304. http://dx.doi.org/10.1007/978-0-387-34866-7_32.
[38] Liu PL, Der Kiureghian A. Optimization algorithms for structural reliability. Struct Saf 1991;9(3):161–77. http://dx.doi.org/10.1016/0167-4730(91)90041-7.
[39] Radwanska Maria. Plate and shell structures : selected analytical and finite element solutions. Chichester, West Sussex, United Kingdom: John Wiley & Sons, Inc.; 2017.
[40] ASM Aerospace Specification Metals. ASM handbooks online. Report, ASM Aerospace Specification Metals, Inc..
[41] Sensitivity analysis. Wiley series in probability and statistics, Wiley; 2000.
[42] Niu X, Wang R, Liao D, Zhu S, Zhang X, Keshtegar B. Probabilistic modeling of uncertainties in fatigue reliability analysis of turbine bladed disks. Int J Fatigue 2021;142:105912. http://dx.doi.org/10.1016/j.ijfatigue.2020.105912.
[43] Abid Fatma, Hami Abdelkhalak El, Merzouki Tarek, Walha Lassaad, Haddar Mohamed. An approach for the reliability-based design optimization of shape memory alloy structure. Mech Based Des Struct Mach 2021;49(2):155–71. http://dx.doi.org/10.1080/15397734.2019.1665541.
[44] Kang Soo-Chang, Koh Hyun-Moo, Choo Jinkyo. Reliability-based design optimisation combining performance measure approach and response surface method. Struct Infrastr Eng 2011;7:477–89. http://dx.doi.org/10.1080/15732479.2010.493335.